CSRME

Contents lists available at ScienceDirect

Journal of Rock Mechanics and Geotechnical Engineering

journal homepage: www.jrmge.cn



Full Length Article

Atomistic origin of montmorillonite clay subjected to freeze-thaw hysteresis



Pengchang Wei ^{a, b}, Zhen-Yu Yin ^b, Chi Yao ^c, Zhifeng Ren ^{d, *}, Yuan-Yuan Zheng ^{a, **}, Wei Ma ^e

- a School of Civil Engineering, Sun Yat-Sen University & Southern Marine Science and Engineering Guangdong Laboratory (Zhuhai), Zhuhai, 519082, China
- b Department of Civil and Environmental Engineering, The Hong Kong Polytechnic University, Hung Hom, Kowloon, Hong Kong, China
- ^c School of Infrastructure Engineering, Nanchang University, Nanchang, 330031, China
- ^d School of Architecture and Energy Engineering, Wenzhou University of Technology, Wenzhou, 325000, China
- e State Key Laboratory of Frozen Soil Engineering, North-west Institute of Eco-Environment and Resources, Chinese Academy Sciences, Lanzhou, 730000,

ARTICLE INFO

Article history: Received 27 June 2024 Received in revised form 3 September 2024 Accepted 7 November 2024 Available online 12 November 2024

Keywords: Frozen soil Freeze-thaw cycles Ultra-low temperatures Molecular dynamics Nuclear magnetic resonance (NMR)

ABSTRACT

The freeze-thaw cycles of frozen soil could significantly affect its thermo-hydro-mechanical-chemical (THMC) properties, causing the frost heaving and thawing settlement. The microscale essence is the water-ice phase transition, but the microscale details are still poorly understood, especially at ultra-low temperatures. Nuclear magnetic resonance (NMR) technology and molecular dynamics (MD) simulation method were performed to explore the freeze-thaw behaviors of montmorillonite clay under temperature of 210-293 K. Then, the water-ice phase transition, freeze-thaw hysteresis, ice nucleation mechanism, and surface effect of clay at an atomistic level were discussed. A classification method of different types of unfrozen water through NMR experiment was proposed, including bulk, capillary, and bound water. Here, it is found that: (1) the freeze-thaw process of frozen soil at the macroscale was essentially the occurrence of ice-water phase transition at the microscale. (2) The freeze-thaw hysteresis was caused by different growth and melting rates of ice crystals, where the ice growth/nucleation on clay surface (i.e. freeze process) was more difficult to develop. (3) The surface effect of clay was essential for the ice nucleation and the existence of bound water. For example, little unfrozen water still existed in unfrozen soil even at 213 K. (4) For unsaturated frozen soil, the quasi-liquid water was an essential component of unfrozen water that cannot be ignored. This work could provide an atomistic insight to unravel the atomistic origin of the freeze-thaw mechanism of montmorillonite clay and complement relevant experimental evidence.

© 2025 Institute of Rock and Soil Mechanics, Chinese Academy of Sciences. Published by Elsevier B.V. This is an open access article under the CC BY-NC-ND license (http://creativecommons.org/licenses/by-nc-nd/4.0/).

1. Introduction

Expansive soil is widely found across more than 60 countries and regions. China has the largest percentage, covering an area of 6.0×10^5 km² (Shi et al., 2002). Expansive soil primarily consists of highly hydrophilic clay minerals like montmorillonite, exhibiting

Peer review under responsibility of Institute of Rock and Soil Mechanics, Chinese Academy of Sciences.

notable deformation properties, such as water absorption expansion and shrinkage (Asuri and Keshavamurthy, 2016). Additionally, the expansive soil in seasonal frozen regions is frequently subjected to freeze-thaw and drying-wetting cycles (Zhao et al., 2021). The temperature-driven water-ice phase transition in frozen soil can significantly impact the water cycle, freeze-thaw behavior, and strength of the soil (Jin et al., 2020; Nan et al., 2022; Wu et al., 2023; Qiu et al., 2024), causing redistribution of water and solutes in surrounding soil, changing pore structure, hydraulic/thermal conductivity, and other thermo-hydro-mechanical-chemical (THMC) properties of frozen soils (Ren et al., 2023a; Wang et al., 2023; Niu et al., 2024), causing frost heaving and thawing settlement in cold region engineering (Fig. 1). Therefore, the freeze-thaw process in

st Corresponding author.

^{**} Corresponding author.

E-mail addresses: 20240102@wzut.edu.cn (Z. Ren), zhengyy57@mail.sysu.edu.cn

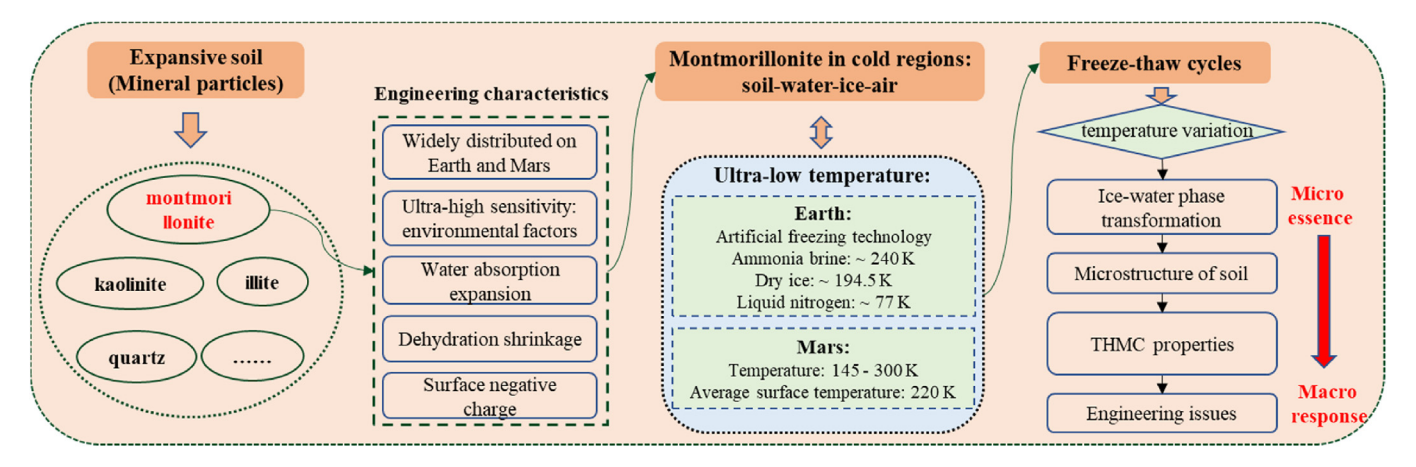


Fig. 1. The freeze-thaw process of frozen soil under temperature variation.

frozen soil plays an essential role in the stability and lifespan of infrastructure, and it contributes to the particularity and complexity of the thermo-mechanical behavior of frozen soils. The microscopic essence of the macroscopic freeze-thaw process in frozen soil is the unfrozen water-ice phase transition (Mironov et al., 2018; Pan et al., 2020; Wei et al., 2024a), while its microscale details are still poorly understood. Based on the complex surface effect of mineral particles, for example, montmorillonite (Mt) is a major component of expansive soil or bentonite with a surface negative charge and strong hydrophilicity properties, and is also one of the common minerals on Earth or Mars (Du et al., 2023). Thus, to explore the atomistic origin of the freeze-thaw process of montmorillonite clay, a strong need remains for understanding the Mt-water-ice interaction, and the surface effect of minerals on water-ice phase transition at ultra-low temperature, particularly in nano-/micro-scale.

Experiments (Svensson and Hansen, 2010; Mironov et al., 2018; Ren et al., 2023a) and theoretical studies (Birgersson et al., 2010; Li et al., 2023; Wang and Hu, 2023; Li and Yin, 2024) could quantify the unfrozen water evolution in frozen soil during the freeze-thaw process, and obtain the soil freezing characteristic curve (SFCC), soil thawing characteristic curve (STCC), and phase composition curves (PCC). However, exploring the formation and fracture of hydrogen bonds and atomic mechanisms in unfrozen water-ice phase transitions through experiments and theoretical studies remained challenging. For example, the phase transition from water to ice typically occurs at a critical nucleus size of ~nm, proceeding very rapidly (ps or ns) (Matsumoto et al., 2002; Sosso et al., 2016b). Thus, the atomistic simulation could provide invaluable insights by elucidating the water-ice phase transition mechanism and its intricate surface effects at the microscale, complementing experimental evidence. The coarse-grained molecular dynamics (MD) simulation method was successfully employed to explore the phase composition behavior of nano-size pores in frozen soils (Zhang et al., 2018), and simulate a larger time and space scale, but ignored the electrostatic interaction between mineral and waterice. All-atom MD simulation method has been effectively investigated the complex physio-chemistry properties of materials (Zheng and Zaoui, 2018; Zhang et al., 2023), such as the bulk ice nucleation process (Matsumoto et al., 2002; Bai et al., 2019) and mechanical behavior of ice (Tulk et al., 2019; Wei et al., 2022a), and ice nucleation process on mineral surface (Cox et al., 2014; Sosso et al., 2016a,b; Zielke et al., 2016; Liang et al., 2023). Furthermore, Wei et al. (2024a) investigated the unfrozen water and ice evolution on the montmorillonite surface at five temperature points (230-270 K). They suggested exploring additional temperature

points, as well as comparing a high-purity montmorillonite sample in an NMR experiment with a montmorillonite crystal model in an MD simulation. However, these previous works did not unravel the water-ice phase transition mechanism on mineral particles with complex surface effects during the freeze-thaw process at the microscale.

To date, the temperature range of 273-243 K in frozen soil mechanics has been widely studied, but there is little research on other ultra-low temperatures (Ren et al., 2023a), which exists in some situations on Earth and Mars (Sebastián et al., 2010) (Fig. 1), such as artificial freezing technology (~194.5 K) and average surface temperature of Mars (~220 K). To unravel the atomistic origin of freeze-thaw process of montmorillonite and complement relevant experimental evidence, NMR experiment was performed to study the unfrozen water evolution and phase composition at ultra-low temperature (~210 K), and all-atom MD simulation method was used to unravel their fundamental mechanism. This paper aims to (1) reveal the water-ice phase transition mechanism on clay surface during the freeze-thaw process; (2) explore the complex surface effect of clay and its effect on water-ice system; (3) propose a microstructure of frozen soil based on double layer theory; and (4) clarify the freezing-thawing hysteresis of frozen soil.

2. Materials and methods

2.1. System setup and force field

The initial unit cell was derived from (Viani et al., 2002) for the Wyoming-type montmorillonite model, with a chemical formula of $Na_{0.75}(Si_{7.75}Al_{0.25})(Al_{3.5}Mg_{0.5})O_{20}(OH)_4 \cdot nH_2O$. After completing the basal spacing changing and lattice substitution, $(4a \times 1b \times 1c)$ Namontmorillonite supercell was obtained from our previous study (Wei et al., 2022b), where cation Na⁺ was used to compensate for the negative charge on montmorillonite surface. Thereafter, $(8a \times 7b \times 2c)$ Na-montmorillonite supercell containing 4565 atoms used in this work is established, as shown in Fig. 2. On the other hand, the unit cell of ice-Ih was derived from (Bernal and Fowler, 1933), with a supercell containing 12,096 atoms. The icevacuum interface was utilized to simulate the ice-air interface, where this processing method was verified in previous work (Weber et al., 2018). The initial Mt-ice system was obtained by merging Na-montmorillonite and ice-Ih model, where the size of whole system is $41.44 \times 62.86 \times 102.973 \text{ Å}^3$ (Figs. 2 and 3a). Thereafter, Mt-water-ice system was obtained after energy minimization and first equilibrium (Equi. 1) for 100 ns at 270 K (Fig. 3a).

As shown in Fig. 2, the bottom around 4 Å layer of the substrate

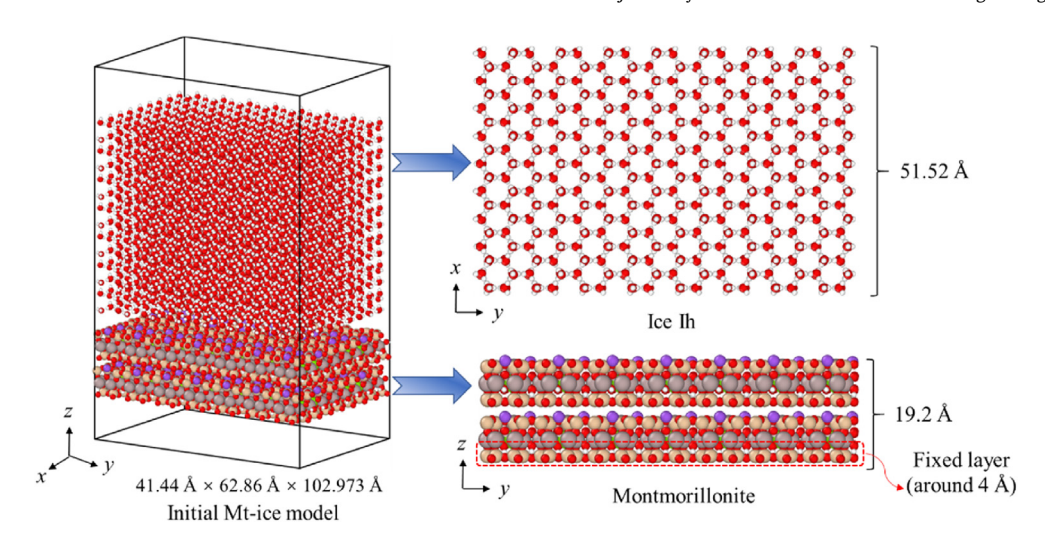


Fig. 2. Initial Montmorillonite-ice (Mt-ice) with 16,661 atoms using in this work, and Mt and ice-lh models containing 4565 and 12,096 atoms, respectively.

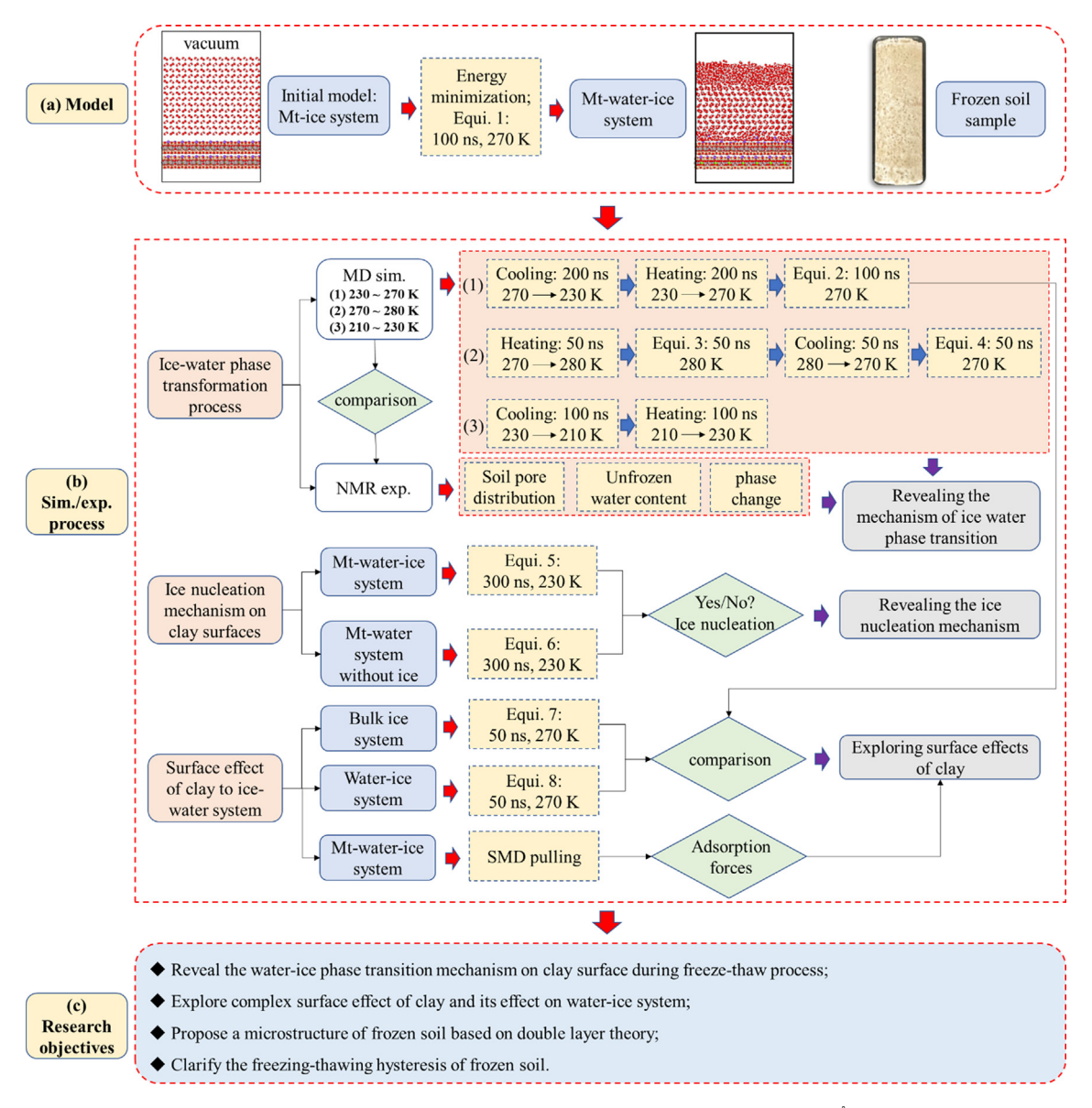


Fig. 3. The MD simulation and experiment flowchart of this work: An initial Mt-ice model with an initial interlayer spacing of 6 Å was established, and a Mt-water-ice model at 270 K was obtained after first equilibrium (Equi.) for 100 ns. Moreover, the frozen soil sample used for NMR experiments is displayed. MD simulation (sim.) and NMR experiment (exp.) process, as well as research objectives of this work are illustrated. Note that Equi. 1 and 2 correspond to the first and second equilibrium process for simplicity, respectively.

is fixed as an immovable layer to ensure the substrate stability without displacement, while the remaining atoms are set as a free layer with an NVE ensemble for time integration. To control the temperature of the whole system, a Langevin thermostat is applied to the atoms in the montmorillonite's free layer.

The CLAYFF force field (Cygan et al., 2004) has been widely employed in MD simulations to study various physio-chemical properties of clay minerals (Yang and Zaoui, 2016; Al-Zaoari et al., 2022; Liu et al., 2024), and was utilized in this work. The TIP4P/ICE rigid water model (Abascal et al., 2005), controlled by the SHAKE method, was applied to describe the water and ice system. This TIP4P/ICE model has been well-validated to accurately reproduce various properties of liquid water and different ice phases, and to study the ice formation behavior on kaolinite surface (Sosso et al., 2016a; Zielke et al., 2016). The melting temperature of this TIP4P/ICE model was obtained as (270 ± 3) K in previous MD studies (García Fernández et al., 2006; Blazquez and Vega, 2022), which agreed well with the experiment value of 273 K. The total potential energy (E_{total}) of whole system was obtained through Eq. (1), and their potential parameters were displayed in Table A1 - 3.

including the following three parts:

- (1) For ice-water phase transformation process, three different temperature ranges (i.e. 210 230 K, 230–270 K, 270–280 K) were divided to explore the supercooling temperature and near the melting temperature states. The cooling-heating processes were used to simulate the freeze-thaw processes of frozen soil, respectively. The temperature of whole system was linearly decreased or increased with a temperature variation rate of 0.2 K/ns. During the first equilibrium (Equi. 1) process, the temperature of whole system was kept unchanged at a target temperature for a period of simulation times. The total simulation time in this part was 900 ns.
- (2) For the ice nucleation mechanism on the clay surface, Mt-water system without ice and Mt-water-ice system were established (see Section 3.6), and they were equilibrated at 230 K for 300 ns, respectively. During the equilibrium process, the ice number, hydrogen bond structure, and total energy of whole system were focused.
- (3) For surface effect of clay to ice-water system, bulk ice and

$$E_{\text{total}} = E_{\text{bond stretch}} + E_{\text{angle bend}} + E_{\text{Coulomb}} + E_{\text{VDW}} = \sum_{i \neq j} k_1 (r_{ij} - r_0)^2 + \sum_{i \neq j \neq k} k_2 (\theta_{ijk} - \theta_0)^2 + \frac{e^2}{4\pi\varepsilon_0} \sum_{i \neq j} \frac{q_i q_j}{r_{ij}} + \sum_{i \neq j} 4\varepsilon_{ij} \left[\left(\frac{\sigma_{ij}}{r_{ij}} \right)^{12} - \left(\frac{\sigma_{ij}}{r_{ij}} \right)^6 \right]$$

$$\tag{1}$$

where σ_{ij} and ε_{ij} are calculated through the Mixing Lorentz-Berthelot's law (Frenkel and Smit, 2001) as follows:

$$\sigma_{ij} = \frac{\sigma_i + \sigma_j}{2} \tag{2}$$

$$\varepsilon_{ij} = \sqrt{\varepsilon_i \varepsilon_j} \tag{3}$$

where k_1 is force constants, and r_0 and r_{ij} represent the equilibrium bond length as well as the distance between atoms i and j, respectively; θ_{ijk} is the bond angle of hydrogen-oxygen-hydrogen, and θ_0 represents the equilibrium bond angle; q_i and q_j are the charges of atoms i and j, respectively; ε_0 is the dielectric constant; σ and ε are the size and energy parameters, respectively.

2.2. MD simulation procedure

All MD simulations are conducted using the LAMMPS (Plimpton, 1995) code, where some setting algorithm and methods for all MD simulations are shown in Table 1. To achieve the research objectives (Fig. 3c) and b shows the MD simulation and experiment process,

water-ice systems were established (see Section 3.7), then equilibrated at 270 K for 50 ns, respectively. These simulation results were discussed with the case of Mt-water-ice system after Equi. 2. Moreover, to study the interfacial interaction between montmorillonite and ice-water, steered molecular dynamics (SMD) pulling along z-direction was conducted in Mt-water-ice system (see Section 3.7) to assess the adsorption force.

Furthermore, the calculation of physical quantities used in this work and their equations are shown in Appendix (Note 1), including order parameter F_3 , mean square displacement (MSD), radial distribution function (RDF), potential energy ($U_{\rm spring}$) and work (W) of virtual spring, and potential of mean force (PMF) and pulling force ($F_{\rm pulling}$). The Open Visualization Tool (OVITO) software (version 3.3.5) (Stukowski, 2010) and Visual Molecular Dynamics (VMD) software were used for visualization.

2.3. Nuclear magnetic instrument and test process

The principle of NMR experiment was displayed in Appendix (Note 2). As shown in Fig. 4, the NMR experiment and its procedure

Table 1Some setting algorithms and methods for all MD simulations and their purposes.

Setting algorithm and methods	Purpose/parameter
Three-dimensional periodic boundary conditions	Simulating the behavior of large systems and improving computational efficiency
SHAKE method for TIP4P/ICE water model	Maintaining molecular structure, improving computational efficiency, and maintaining dynamic
	characteristics
Velocity Verlet algorithm	Integrating the motion equations
Lennard-Jones potential model, with a cut-off radius of 10 Å	Calculating the van der Waals interaction
PPPM/TIP4P method, with a cut-off radius of 8 Å	Calculating the long-range electrostatic interaction
Time step	1.0 fs

NMR experiment process

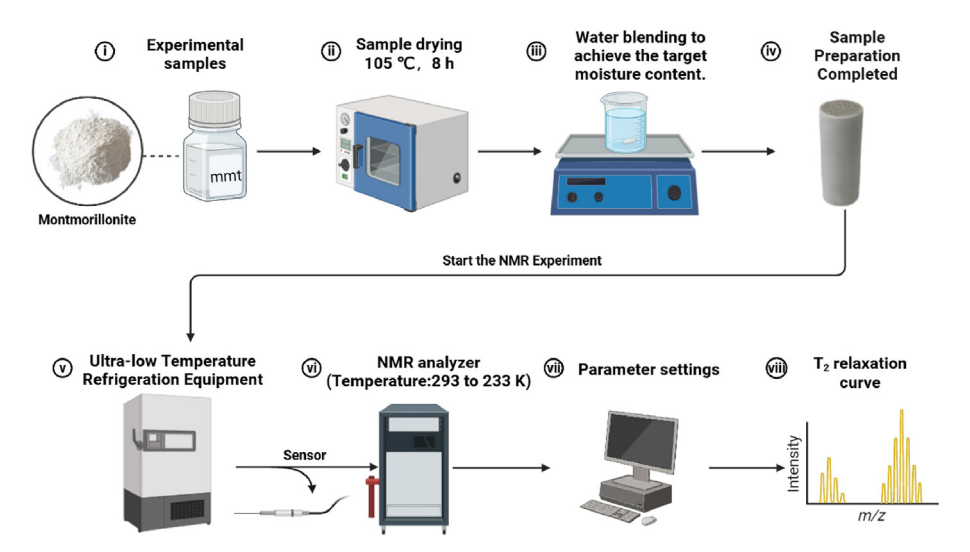


Fig. 4. NMR experiment process and data processing analysis.

are as follows:

- (1) Sample preparation involved pure montmorillonite, characterized by a melting point of 337-340 K, a density of 2.3-2.5 g/cm³, a molecular weight of 282.2, and a powdered, layered molecular structure. The montmorillonite was placed in a 378 K oven for 8 h to remove its natural moisture content. Based on the designed moisture content and dry density, a specific mass of montmorillonite and water was measured, uniformly mixed, and pressed into a specialized polytetrafluoroethylene mold. Care must be taken during sample preparation to control the soil quantity and static pressure. The mold was then placed in a saturation tank with filter paper and permeable stone pressed on both ends for 12 h soaking. After wrapping with plastic wrap and sealing in a bag, the sample was left to stand and saturate for 24 h to ensure uniform water distribution throughout the soil. The initial moisture content was measured at this point.
- (2) The prepared soil sample was placed in an NMR instrument, and a cold bath device was employed to control its temperature. The freezing temperatures were set to 293 K, 283 K, 278 K, 273 K, 272.9 K, 272.8 K, 272.7 K, 272.5 K, 272.3 K, 272 K, 271 K, 270 K, 269 K, 268 K, 263 K, 253 K, 243 K, 233 K, 223 K, and 213 K. The temperatures from 293 K to 233 K were controlled using the NMR's built-in cooling system, and temperatures from 233 K to 213 K were controlled using an ultra-low temperature freezer. Dense temperature points were set in the phase transition region. The system was equipped with a temperature monitoring device, and signals were collected after reaching the target temperature and maintained for 1 h. The temperature range for the thawing process is the reverse.
- (3) The conditions for the NMR experiment were set as follows: Carr-Purcell-Meiboom-Gill (CPMG) RF sequence, sampling frequency of 250 kHz, analog gain of 15,3000 echoes, echo time of 0.15 ms, and waiting time of 1000 ms. The NMR signals collected at the target temperatures were then inverted and calculated to obtain the T₂ (transverse relaxation time) relaxation curve and peak area. The peak area is converted to unfrozen water content using the Tice method,

which relies on the proportional relationship between water molecule content and NMR signal.

3. Results

3.1. Unfrozen water evolution from NMR experiment

The main findings from NMR experiment were obtained as follows:

- (1) These curves in Fig. 5a, b exhibit a single peak structure and follow a normal distribution, indicating uniform sample preparation with no large pores. The larger the area enclosed by the T₂ curve and the horizontal axis, the higher the liquid water content (Anderson and Tice, 1972; Ren et al., 2023a). The unfrozen water content rises exponentially with increasing temperature during the freeze-thaw process (Fig. 5c), where it significantly changes during severe and transitional phase-transition zones (Kong et al., 2020; Ren et al., 2023b). Moreover, unfrozen water still existed because of the strong surface effect of soil particles even at ultra-low temperatures. More details please see Appendix (Notes 3, 4).
- (2) The freezing-thawing hysteresis characteristic curve (Tian et al., 2014) was found in Fig. 5c because SFCC and STCC did not overlap, forming a closed hysteresis loop. Moreover, the freezing-thawing hysteresis characteristic curve can be divided into four stages, which will be discussed in Section 3.2.
- (3) Unfrozen water content at different temperatures can be calculated by determining their respective area shares, where unfrozen water content corresponds to the sum of gravitational, capillary, and bound water (Fig. 5d). We precisely identified different types of unfrozen water at various temperatures (see Section 3.2). At 271–273 K, the unfrozen water content is equal to the initial water content, as the soil remains in an unfrozen state. At 270 K, freezing of the soil initiates, resulting in a decrease in the content of bulk, capillary, and bound water. It is observed that gravitational water is completely frozen at 270 K, capillary water at 268 K,

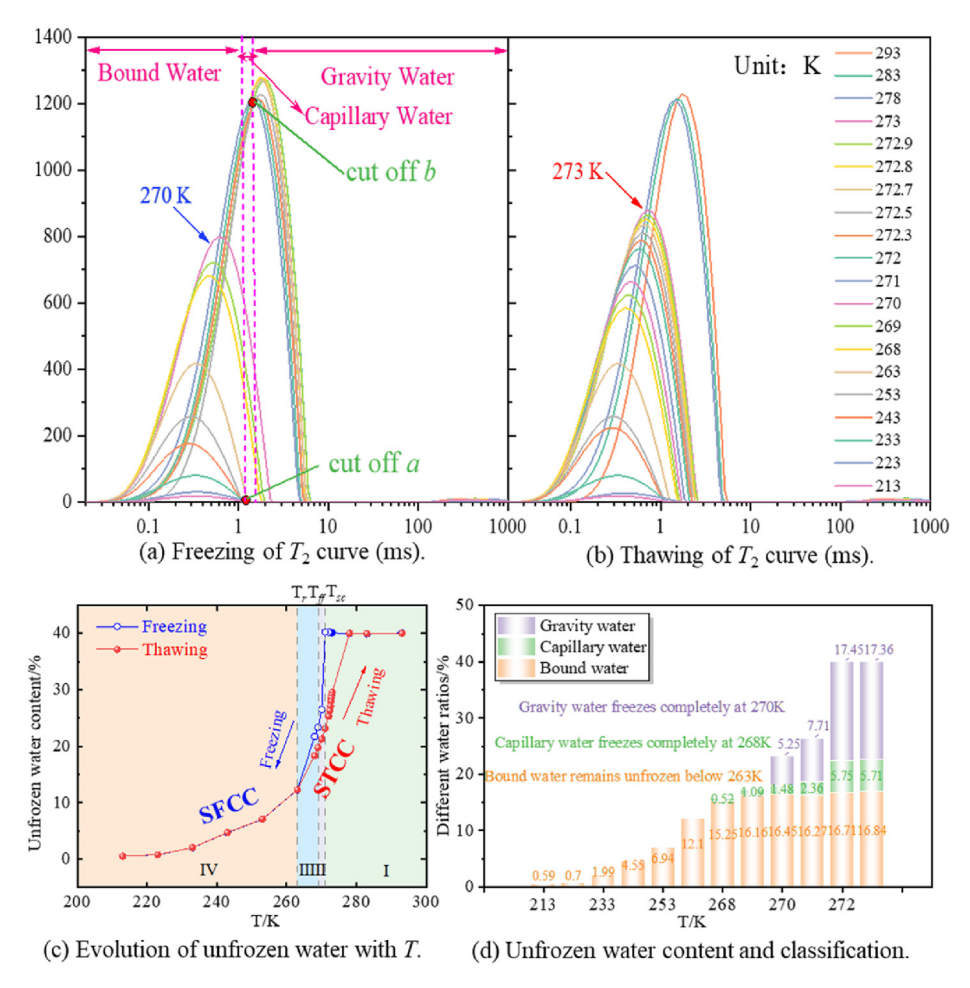


Fig. 5. The determination of unfrozen water in frozen soil through NMR experiment. T_2 relaxation curve during (a) freezing and (b) thawing process. (c) Evolution of unfrozen water with temperature under freez-thaw process (i.e. Soil Freezing Characteristic Curve (SFCC) and Soil Thawing Characteristic Curve (STCC)), where T_{sc} represents the metastable undercooling temperature relative to thermodynamic equilibrium; T_{ff} is the temperature at complete freezing of free water; and T_r corresponds to the temperature at which the residual unfrozen water content is achieved. (d) Unfrozen water content and its classification at different temperatures.

and below 263 K, only bound water remains unfrozen. Even at 213 K, a little bound water remains.

3.2. Freezing-thawing hysteresis characteristic curve

As shown in Fig. 5c, based on the characteristics of unfrozen water content during the freez-thaw process, the freezing-thawing hysteresis characteristic curve can be divided into four stages:

- (1) Phase I: In the freezing characteristic curve, the unfrozen water content remains constant as temperature decreases; while in the thawing curve, the unfrozen water content gradually increases as the temperature rises. When the temperature reaches the freezing point of free water, most of the pore ice in the soil-water system melts, and the unfrozen water content remains constant as the temperature continues to rise. In Phase I, as the temperature decreases, the hysteresis degree of unfrozen water content in the freezthaw process gradually increases.
- (2) Phase II: In the freezing characteristic curve, the unfrozen water content dramatically decreases as the temperature drops, with all free water in the soil-water system's pores transforming into ice. Conversely, in the thawing

- characteristic curve, the unfrozen water content rapidly increases as temperature rises. Ice in small- and medium-sized pores completely melts, leaving only a small amount of ice crystals unfrozen in large pores. In Phase II, as the temperature decreases, the overall hysteresis degree of unfrozen water content in the freez-thaw process remains stable.
- (3) Phase III: During the freezing process, as the temperature further decreases, the thin film water in the pores begins to transform into ice, leading to a decreasing rate of unfrozen water content with decreasing temperature. In the thawing process, the unfrozen water content gradually increases as temperature rises, with ice crystals in small pores completely melting and a significant amount of ice crystals in medium to large pores beginning to melt, causing an increased rate of unfrozen water content with temperature. In Phase III, as temperature decreases, the overall hysteresis degree of unfrozen water content in the freez-thaw process gradually decreases.
- (4) Phase IV: In the freezing characteristic curve, gravity water and capillary water in the soil-water system freeze entirely, leaving only bound water unfrozen. In Phase IV, the unfrozen water content in the freez-thaw processes is essentially equal, and the hysteresis degree of unfrozen water content in the freez-thaw process is approximately 0.

3.3. Classification of unfrozen water under various temperatures through NMR experiment

In soil, water distribution can be classified into three types: gravitational water, capillary water, and bound water. Using nuclear magnetic resonance (NMR) technology, the T₂ distribution curve reveals a threshold on the transverse relaxation time. When the transverse relaxation time of water in the soil pores is greater than a threshold value, the fluid is classified as capillary water. Otherwise, it is bound water. This critical transverse relaxation time is known as the fluid T₂ cutoff value, and its determination is crucial for distinguishing water types (Chen et al., 2021), showed that water with different pore size distributions has different transverse relaxation times T₂. Specifically, in Fig. 5a, when the temperature ranges from 293 K to 272 K, the T₂ curve slightly intersects to the left of the peak at 1.38. This intersection, termed cutoff-b, lies between gravitational water and capillary water. The point where the T₂ curve intersects x-axis without further shifting is cutoff-a. Despite the gradual decrease in pore water volume, this type of pore water and its energy remain constant. Cutoff-a (1.2) serves as the boundary between gravitational water and bound water.

Based on the above analysis, by calculating the T_2 relaxation curve shown in Fig. 5a, we can use two cutoff values to distinguish bulk, capillary, and bound water. However, the T_2 relaxation curve only provides the distribution of these water types, without

indicating their respective amount. To address this we correlate the NMR signal with the unfrozen water content in the pores. By classifying T_2 relaxation curves at the same temperature based on cutoff values, we calculate the enclosed area of these curves within a specified range of the horizontal axis.

3.4. Ice-water phase transition process in MD simulation

As shown in Fig. 6a—d, the initial Mt-ice model without water could transform into Mt-water-ice system for 100 ns at 270 K, where the structure of some ice molecules is destroyed under thermo-loading. Thereafter, during the cooling (from 270 K to 230 K) process, the evolution of unfrozen water transforming into ice is rapid in 270—258 K, and is slow in 258—230 K. During heating (from 230 K to 270 K) process, it was opposite to the cooling process, where the ice molecules transformed gradually into water molecules. It indicated that the ice-water phase transformation in frozen soil during freezing-thawing process was reversible. After the heating-cooling process, Mt-water-ice system was further equilibrated for 100 ns at 270 K, and its structure remained almost unchanged (see Fig. 6c and d). Moreover, the ice-water phase transition process at 210—230 K and 270—280 K were discussed in Appendix (Note 5) and Figs. A2 and A3.

Freezing-thawing hysteresis is also found in MD simulation (Fig. 7a), where the unfrozen water content during freezing is

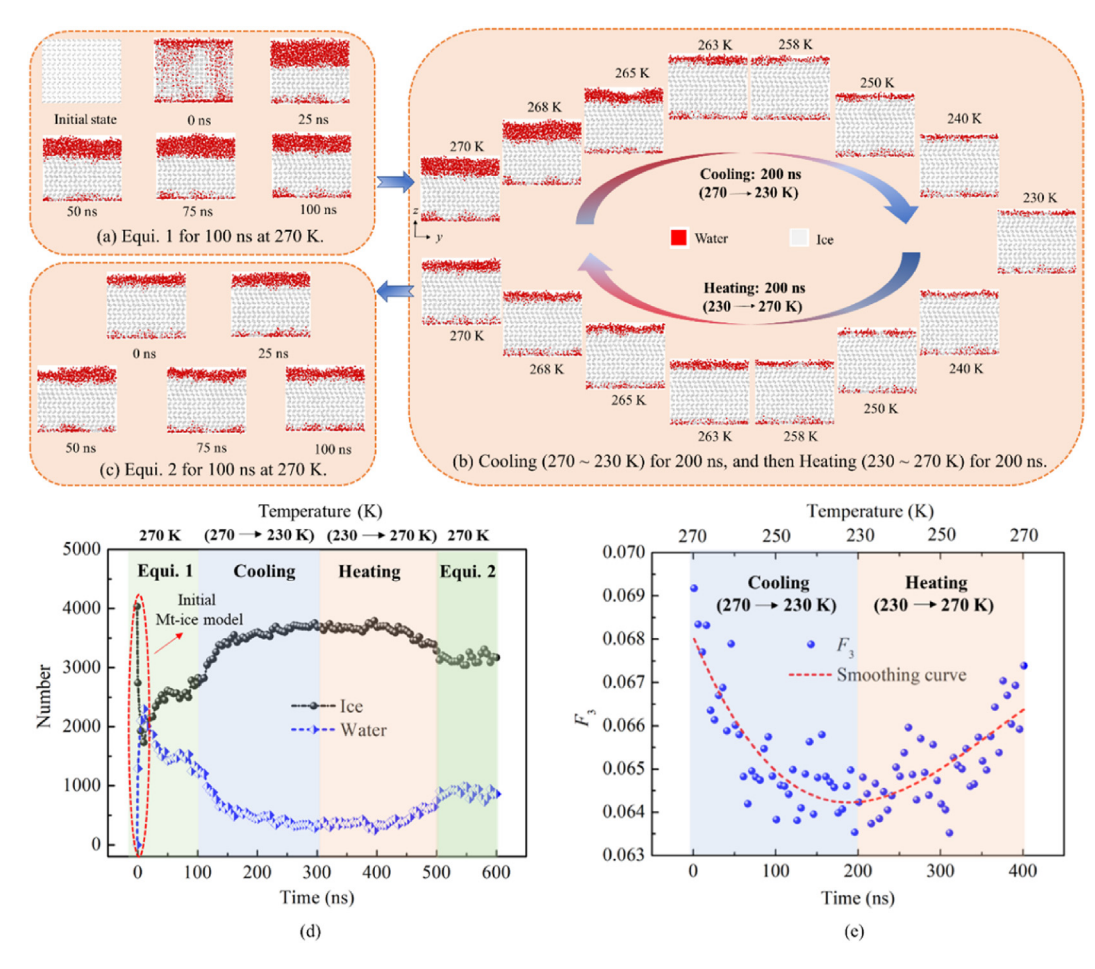


Fig. 6. Ice-water structure in whole system during 230–270 K at different stages: (a) Firstly, initial Mt-ice system equilibrates (Equi. 1) for 100 ns at 270 K. (b) Secondly, the Mt-water-ice system is during cooling (270 - 230 K) and heating (230–270 K) process. (c) Thirdly, the whole system further equilibrates (Equi. 2) for 100 ns at 270 K. Note: For better visual clarity, the montmorillonite system is hidden. A structure identification algorithm proposed by (Maras et al., 2016) in OVITO is applied to determine the distinction between ice and water structure. Moreover, the time and temperature-dependent evolution of (d) the number of ice and water molecules, and (e) the order parameter (*F*₃) in the Mt-water-ice system are analyzed during the heating-cooling process.

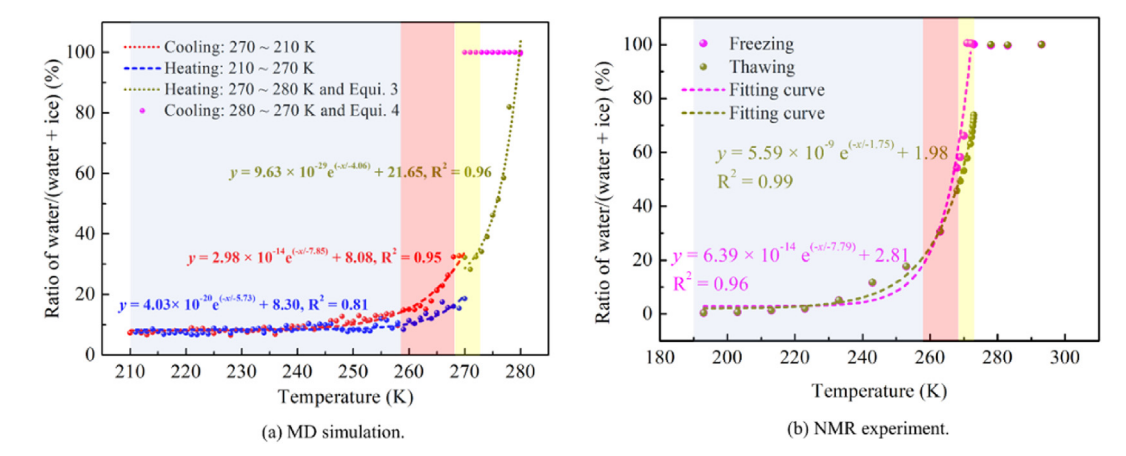


Fig. 7. Evolution of ratio of water/(water + ice) with temperature during different stages from (a) MD simulation and (b) NMR experiment, where fitting curves were obtained fitting from 213 to 273 K. Furthermore, according to the previous studies obtained from (Tsytovich, 1975), frozen soil exhibits three main phase-transition zones: severe phase-transition zone (269–272 K, yellow zone), transitional phase-transition zone (258–268 K, pink zone), and freezing stable zone (<258 K, blue zone).

higher than that in thawing stage (Fig. 5c). Moreover, the MD simulated evolution of unfrozen water with temperature aligns with NMR experimental results (Fig. 7), verifying the accuracy of MD simulation. It was noted that NMR experiments and MD simulations both obtained the exponential functions, but their function parameters were different due to differences in scale effect, model and parameterization, and time scale. As shown in Fig. 8a, the Mtice-water system contains two types of hydrogen bonds (HBonds) (Wei et al., 2024a): water-water (W-W) and clay-water (C-W) HBonds. As shown in Fig. 8b, at 230–270 K, the number of W-W HBonds decreases with rising temperature. The higher temperature could lead to more violent thermal fluctuations of atoms, causing more HBonds to break. However, the number of C-W HBonds remained unchanged all the time.

3.5. Structural and dynamical properties of ice-water and cations

3.5.1. Ice-water system

As shown in Fig. 9a, the ice-water system on clay surface can be divided into three zones: bound water, ice, and quasi-liquid water, where their identification and validation are determined in previous work (Wei et al., 2024a). At 230-270 K, the maximum displacement of atoms was conducted in a quasi-liquid water zone, followed by a bound water zone, but the atoms in the ice zone hardly moved (Fig. 9a and b). At 270-280 K, water molecules in quasi-liquid water zone melt firstly, and then are gradually affected the ice zone (Fig. 9c), where HBonds in whole system break from top to bottom (Fig. 8c). As shown in Fig. 10a and b, MSD along xdirection is close to that along y-direction, and they are significantly greater than that along z-direction, reflecting that ice/water molecules in whole system move basically in horizontal direction. Moreover, the diffusion coefficient increased with rising temperature, and the diffusion coefficient during cooling is greater than that during heating (Fig. 10c). The dynamic properties of frozen soil are closely related to unfrozen water content, where the higher temperature leads to an increase in the unfrozen water content, causing a higher dynamic ability (Fig. 10c and 7a).

To understand the effect of temperature changes on the structural properties of ice-water system, the Radial distribution function (RDF) of O_{TIP4P/ICE}-O_{TIP4P/ICE} and O_{TIP4P/ICE}-H_{TIP4P/ICE} at some different temperatures during heating-cooling process were discussed. As shown in Fig. 11, at 230–270 K, RDF of O_{TIP4P/ICE}-O_{TIP4P/ICE} and O_{TIP4P/ICE}-H_{TIP4P/ICE} contains many obvious peaks at long distances, showing long-range order properties, which is due to the

ice-water system that contains numerous ice molecules. However, at 280 K, Mt-water system without ice illustrated a short-range order and long-range disorder properties (see Fig. 11b, d). On the other hand, as shown in Fig. 11, the first peak value of RDF of $O_{TIP4P/ICE}$ and $O_{TIP4P/ICE}$ -H $_{TIP4P/ICE}$ decreases with increasing temperature. Moreover, compared with other temperatures (i.e. 230 - 260 K), the number of RDF peak $O_{TIP4P/ICE}$ -O $_{TIP4P/ICE}$ and $O_{TIP4P/ICE}$ -ICE-H $_{TIP4P/ICE}$ at 270 K and 280 K reduced, this was due to the high temperature that the more the unfrozen water content, the lower the spatial correlation and long-range order properties for ice-water system.

At 210–250 K, the relatively small thickness of bound water and quasi-liquid water zones lead to a uniform distribution of layers in the overall density distribution of O_{TIP4P/ICE} system (see Fig. 12a–c). At 270 K and 276 K, the quasi-liquid water zone has a density of around 1.0 g/cm³ (i.e. the density of bulk water) when its thickness increases (Fig. 12d and e). Furthermore, as shown in Fig. 12f, at 280 K, for Mt-water system without ice and based on electrical double layer theory, the whole water layer on montmorillonite surface could be divided into three layers as stern layer, diffuse layer, and bulk solution. The density of stern layer was around 1.6 g/cm³, and the density of Diffuse layer with an obvious peak rapidly decreased, while that of bulk solution density was around 1.0 g/cm³. This MD result was consistent with previous MD study (Zhang and Pei, 2021) that finds this distribution for Mt-water system in MD simulations and experiments.

3.5.2. Cations

The space distribution evolution of cations during the heatingcooling process is shown in Fig. 13, where the Na⁺ cations in Mtice-water system are divided into surface and interlayer cations (Fig. 13a). The interlayer cation between two clay sheets hardly moved during heating and cooling process, so the surface cation was mainly discussed in this work. As shown in Fig. 13a and b, the displacement of surface cations at 230-270 K is relatively small, and the surface cations mainly move in the bound water zone and cannot move into the ice zone (Fig. 12a-e). As shown in Fig. 13c, at 270-280 K, some surface cations gradually move upwards and away from clay surface when all ice molecules transform into water with increasing temperature. It was noted that most cations remained on montmorillonite surface due to its strong adsorption. On the other hand, as shown in Fig. 13d, during cooling and Equi. 4 process, the surface cations move downwards and approach montmorillonite surface when the temperature reduces. To sum

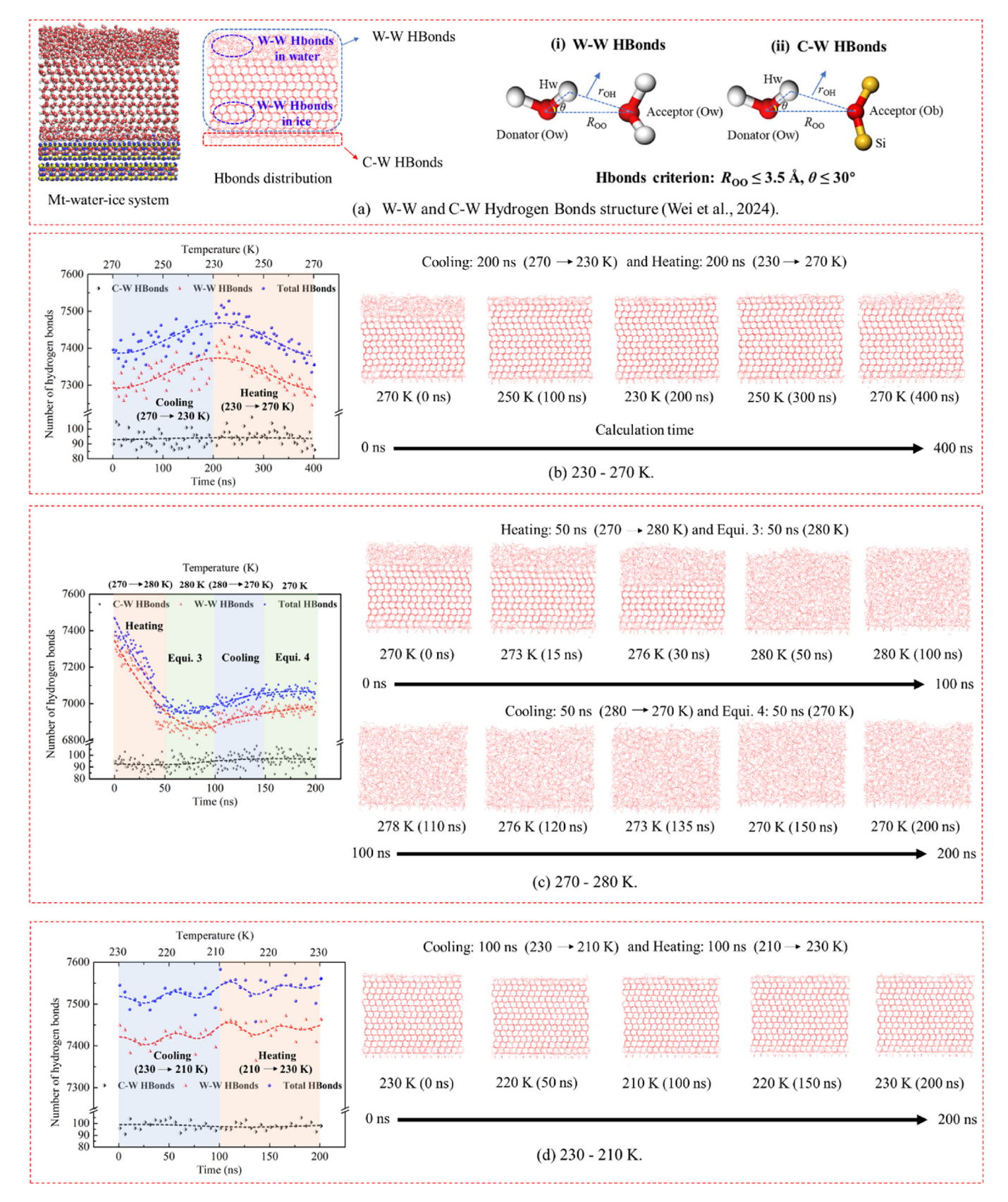


Fig. 8. (a) Schematic diagram of two type of hydrogen bonds (i.e. W-W and C-W HBonds) from (Wei et al., 2024a). (b-d) Hydrogen bonds structure diagram and the evolution of the number of HBonds with time and temperature during heating and cooling process at (b) 230–270 K, (c) 270–280 K, and (d) 230–210 K.

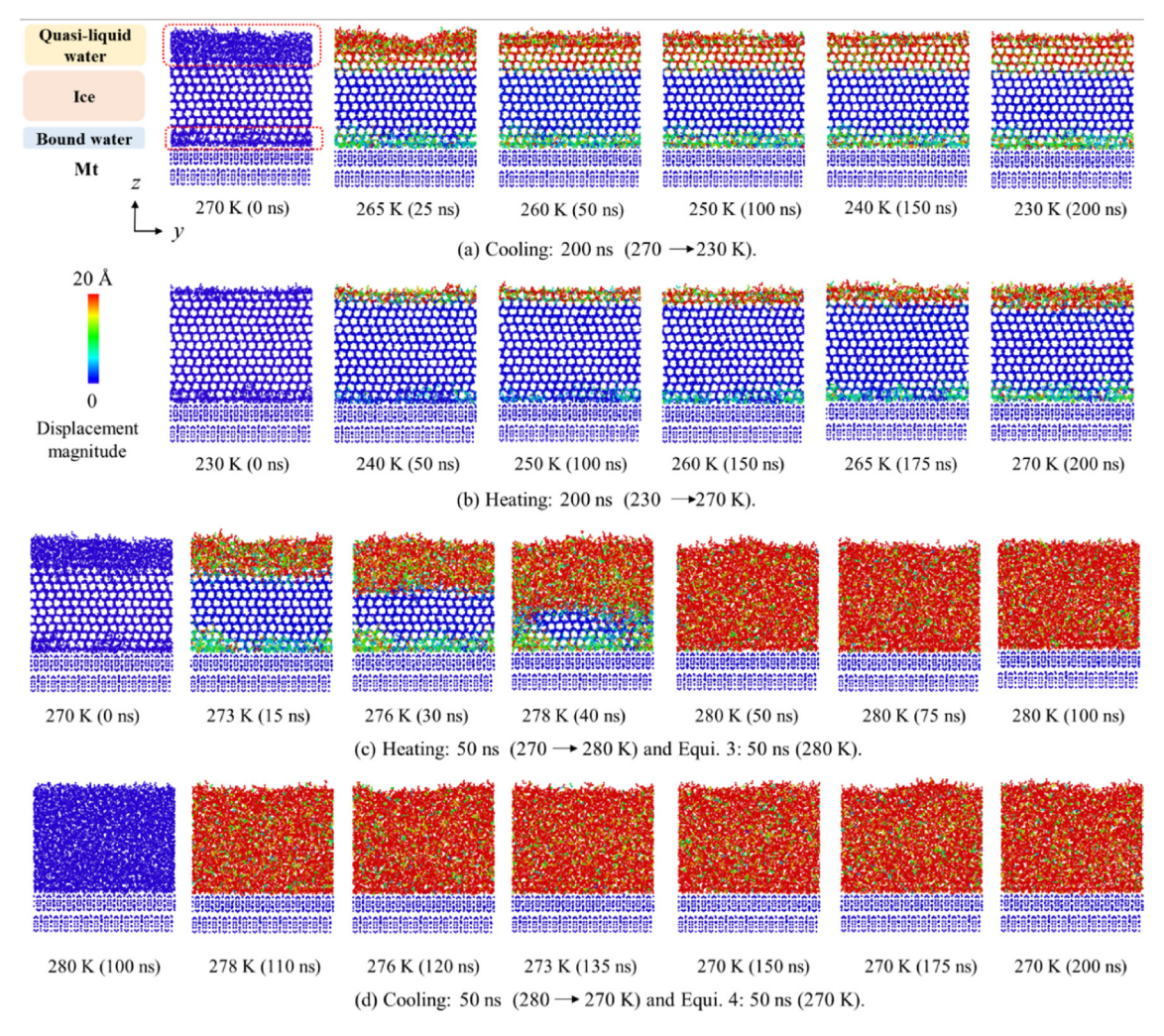


Fig. 9. (a-d) Displacement of all atoms in Mt-water-ice system at various temperatures during heating and cooling process.

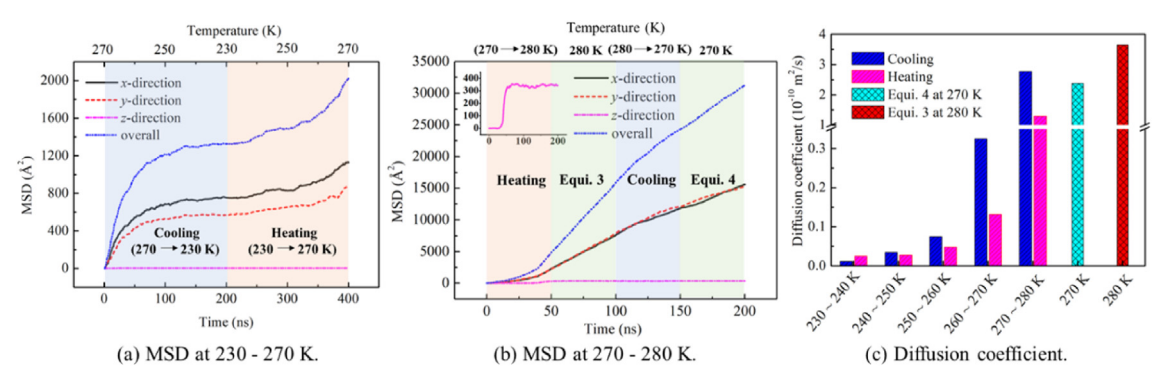


Fig. 10. (a–b) Evolution of MSD of the oxygen atom ($O_{\text{TIP4P/ICE}}$) with time and temperature during (a) 230–270 K and (b) 270–280 K. Moreover, (c) the evolution of its diffusion coefficient ($10^{-10} \text{ m}^2/\text{s}$) with temperature during the heating and cooling process.

up, partial surface cations could break free from the binding/adsorption of montmorillonite, and move into free water area at a temperature exceeding the melting point. These findings could be inferred that ions in the frozen soil could precipitate and leave the soil particle surface during freezing-thawing processes, respectively.

Fig. 14 displays the MSD and diffusion coefficient of cation atoms at different stages, where the value of MSD along three directions $\frac{1}{2}$

during 0–40 ns is very small, then gradually increases with rising time from 40 ns to 200 ns. MSD along z-direction is less than that along x- and y-direction, illustrating that the cation moves mainly in the horizontal direction. Fig. 14b shows the diffusion coefficient of cation at 50–200 ns is superior to that at 0–50 ns, where it is the highest at Equi. 4 process in 270 K, corresponding to the cations moving the montmorillonite surface downwards (Fig. 13d).

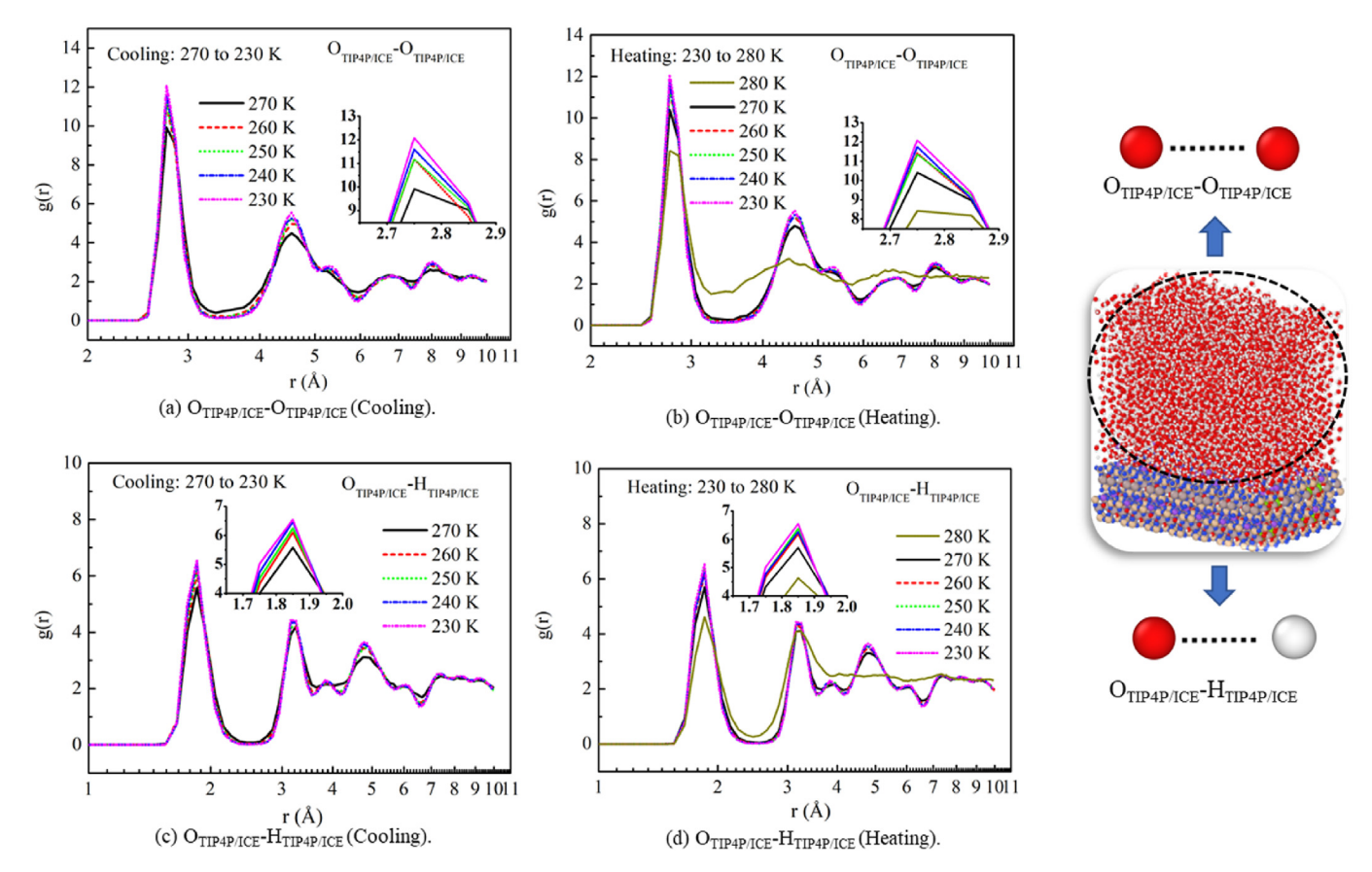


Fig. 11. RDF of different atom pairs during the heating and cooling process: (a, b) $O_{TIP4P/ICE}$ - $O_{TIP4P/ICE}$, and (c, d) $O_{TIP4P/ICE}$ - $H_{TIP4P/ICE}$ atom pairs.

3.6. Ice nucleation mechanism on montmorillonite surface

Freezing water into ice required a temperature below the freezing point and the presence of crystallization nuclei, which could be a small ice crystal, dust particles, suspended particles, and solid surfaces. For Mt-water system, there is no ice crystals formed during 300 ns in Equi. 5 (Fig. 15a), and the total energy of whole system remains unchanged (Fig. 15c). Moreover, all water molecules in whole system have high fluidity even at 270 K (Fig. 9d), indicating that it is difficult to freeze. Based on previous works (Cox et al., 2014; Sosso et al., 2016b; Zielke et al., 2016), the ice nucleation may occur in Mt-water system (Fig. 15a), but it must require more simulation time, like several milliseconds. Alternatively, we can also reduce the size of whole system to save simulation time, which could be conducted in next step.

For Mt-water-ice system with little ice crystals, more and more water molecules could transfer into ice molecules (Fig. 15b–d), and the total energy gradually decreases with rising simulation time (Fig. 15c). It can be inferred that the phase transition of water into ice for Mt-water-ice system can develop as a stable Mt-water-ice structure (Fig. 6b at 230 K) if there is enough simulation time. To sum up, a small amount of ice crystals in whole system as crystallization nuclei played a critical role in ice nucleation on montmorillonite surface.

3.7. Surface effect of montmorillonite to ice-water

The work of adhesion (W_{AB}) (Clancy and Mattice, 1999) is defined as a work that requires two phases to separate from each other, either a liquid-liquid or liquid-solid interface. In this work, the work of adhesion between the water-ice system and the

montmorillonite surface could be obtained by Wei et al. (2024a):

$$W_{AB} = \frac{(E_{\text{water-ice}} + E_{\text{Mt}}) - E_{\text{Mt-water-ice}}}{2A}$$
 (4)

where $E_{\text{Mt-water-ice}}$, E_{Mt} , and $E_{\text{water-ice}}$ are the total potential energy of the whole Mt-water-ice system, bulk montmorillonite system, and water-ice system, respectively. A is the contact area between montmorillonite and water-ice system.

The adsorption force between montmorillonite surface and icewater system comprised van der Waals and coulomb electrostatic force. It could be measured by steered molecular dynamics (SMD) pulling along z-direction, where the SMD simulation method was one of the non-equilibrium MD simulations (Wei et al., 2024b,c). As shown in Fig. 16a, a virtual spring with a stiffness coefficient of 100 N/m is employed to select rigid groups of atoms in whole system along z-direction. The pulling force and PMF could be obtained during SMD simulation process, and effectively reflect the adsorption interaction between montmorillonite and ice-water system.

The maximum pulling force and PMF decrease with rising temperature (Fig. 16c and d), indicating the lower the adsorption force and the resistance to pulling deformation for their interface. It was noted that the evolution of pulling force, PMF, and total energy in 280 K is different from that in other temperatures, because of the difference in structural configuration (Fig. 16b). More water molecules are adsorbed by montmorillonite surface in 280 K during the pulling process, even showing a liquid bridge (Fig. 16b), but only one layer of bound water remains in 210–276 K (Fig. 16a–A4). As shown in Fig. 17, the work of adhesion of Mt-water-ice system (approximate solid-solid interface) in 210–276 K are close, and is

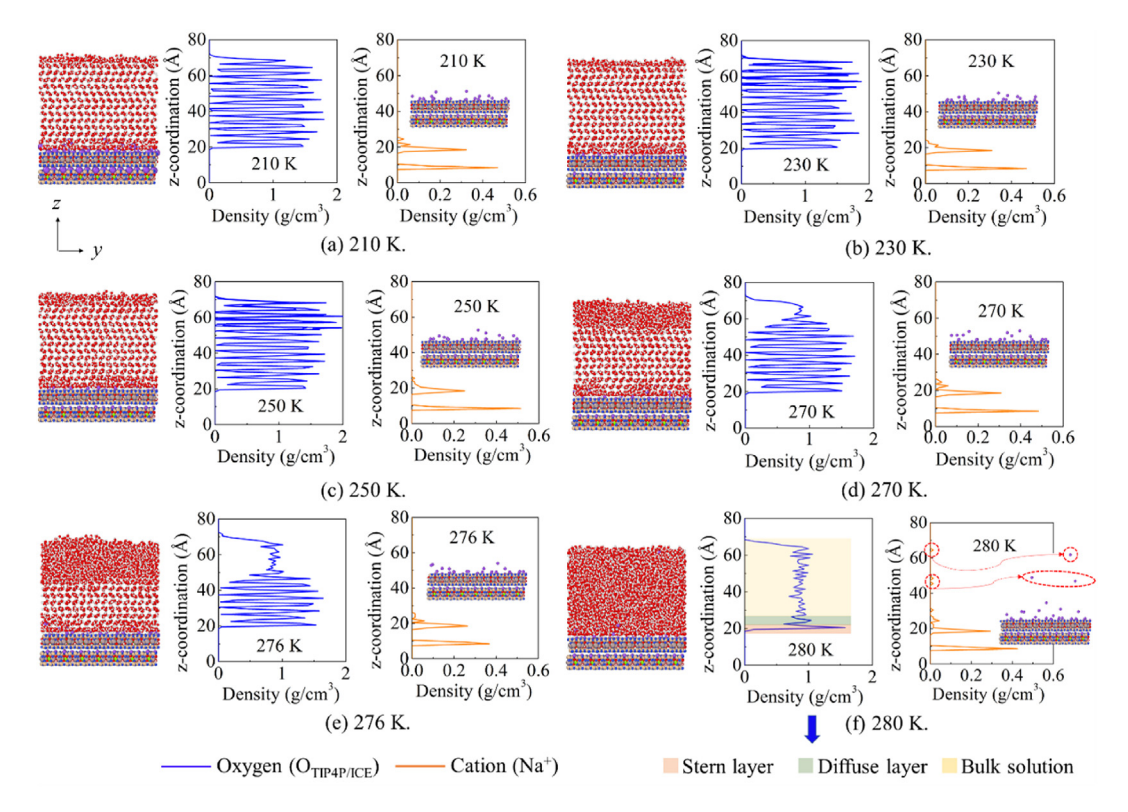


Fig. 12. Density distribution of $O_{\Pi P4P/ICE}$ in ice-water system and cation (Na⁺) at various temperatures: (a–f) 210–280 K. Moreover, (f) combined with the electrical double layer theory.

less than that of Mt-water system (solid-liquid interface) in 280 K, showing lower adhesion for solid-solid interface. Moreover, the interfacial interaction between montmorillonite and water-ice film was a non-bond interaction, where the contribution of coulomb electrostatic interaction was significantly greater than the van der Waals interaction, illustrating that the coulomb electrostatic interaction was the dominant. Furthermore, the surface effect of clay was also reflected in its potential energy surface (Fig. A5), which was significantly important in the presence of bound water on clay surface. To further investigate the surface effect of montmorillonite on ice-water system, bulk ice, water-ice, Mt-water-ice systems are established for relaxation at 270 K for 50 ns (Fig. 18a–c). Without clay adsorption, the water-ice system (Fig. 18b) contains more quasi-liquid water near vacuum, so it has higher liquidity and kinetic energy (Fig. 18d and e).

4. Discussion

4.1. Ice-water phase transition mechanism during the freeze-thaw process

The evolution of unfrozen water with temperature and their function relationship in MD simulation and NMR experiment are consistent, where unfrozen water increases exponentially with rising temperature in severe and transitional phase-transition zones, but remains unchanged in the freezing stable zone (see Fig. 7). The accuracy of the proposed model and force field used in MD simulation could be verified. Moreover, MD study is employed to unravel the atomistic origin of freeze-thaw process of frozen soil, concerning hydrogen bonds variation, which could complement relevant experimental evidence (Fig. 5).

As shown in Fig. 19a, during thawing process, frozen soil gradually absorbs external energy with rising temperature, causing the higher thermal fluctuations of atoms. Thus, the network of hydrogen bonds of whole system is easily prone to breakage, and then ice molecules gradually transits into water molecules, causing higher unfrozen water content. Moreover, the adsorption force between clay and water-ice system gradually reduces with rising temperature, and the liquidity of unfrozen water and cation in whole system increases, where a small number of cations detach from clay's surface adsorption. However, the above case of freezing is opposite to the thawing process.

4.2. Freezing-thawing hysteresis

The ice-water phase transformation in frozen soil during freezthaw process was reversible, while there is a freezing-thawing hysteresis (see Section 3.2) at relatively high temperatures over 260 K (Fig. 5c and 7a), which is also found in previous works (Tian et al., 2014). Because the freez-thaw process in frozen soil corresponded to two different thermodynamic stages, due to the different growth and melting rates of ice crystals, the water transforming into ice during the freezing process was more difficult than the ice transforming into water during the thawing process. Based on this study (see Fig. 15) and previous works (Cox et al., 2014; Sosso et al., 2016b; Zielke et al., 2016), the ice nucleation and growth on clay surfaces usually have higher requirements, such as nucleation time, temperature, and crystallization nuclei.

The transformation of water into ice involves two stages: the formation of nuclei and the growth of ice crystals. When the temperature of the soil rapidly decreases to the freezing point of pure water (273 K), pore water does not freeze immediately; instead, it requires a certain energy reserve. Before crossing the free energy barrier, the pore water remains in a metastable state until the temperature decreases to a certain degree, so that nuclei can form in large quantities. As temperature further decreases, water

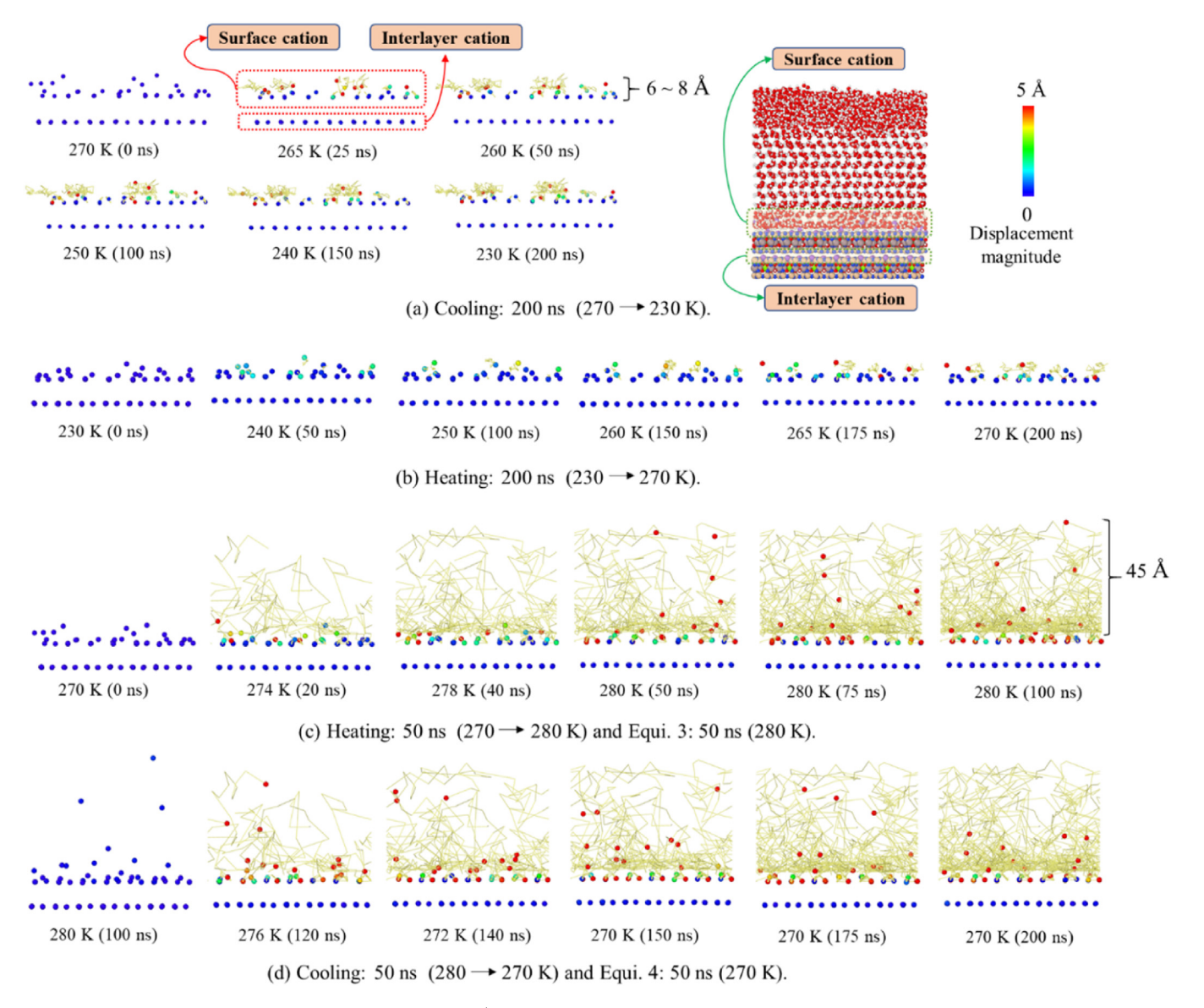


Fig. 13. (a–d) Atom trajectory lines of surface and interlayer cation (Na⁺) at different times and temperatures during the heating and cooling process. The cation atoms in whole system are only shown, and other atoms are hidden for better visual clarity.

molecules around nuclei larger than the critical size gather significantly, leading to rapid nucleation and ice crystal growth. Due to the nucleation effect, at the initial stage of the freezing process, the cooling device primarily affects the formation of nuclei in the pore solution of the soil-water system and the growth of ice crystals. The liquid water content remains essentially unchanged before substantial ice crystal growth occurs. Near temperatures slightly below 273 K, the unfrozen water content remains constant, and the freezing characteristic curve in this temperature range appears as a horizontal line. In other words, the nucleation effect delays the decrease in unfrozen water content in the pore solution of the soilwater system during the freezing process, maintaining the unfrozen water content equal to the initial water content within a certain negative temperature range, a phenomenon known as supercooling.

During the heating-melting process, as there is always a thin layer of liquid water film on the pore wall surfaces of the frozen soil, and the melting of pore ice is a gradual process that does not require a buildup of heat to trigger. Unlike the critical

"superheating" phenomenon observed during the freezing process, when the temperature of the soil reaches 273 K, all the pore ice has already melted. The melting curve shows an increase in unfrozen water as the temperature rises throughout the negative temperature range, coinciding with the freezing curve at 273 K. Therefore, when the temperature of the soil-water system is slightly below 273 K, the unfrozen water content during the freezing process is significantly higher than that during the melting process, indicating a lag in the unfrozen water content.

4.3. Surface effect of clay and phase composition of frozen soil

For unsaturated frozen soil containing air (i.e. region A), the microstructure of water-ice on clay from inside to outside is termed as "clay-bound water-ice-'quasi-liquid' water-air" (Fig. 19a). The appearance of quasi-liquid water on ice surface is found in our MD simulation (Fig. 9a and 6a-c)) and has been verified through experiments (Furukawa et al., 1987; Smit and Bakker, 2017; Kawakami et al., 2020). The quasi-liquid water refers to as a thin water film

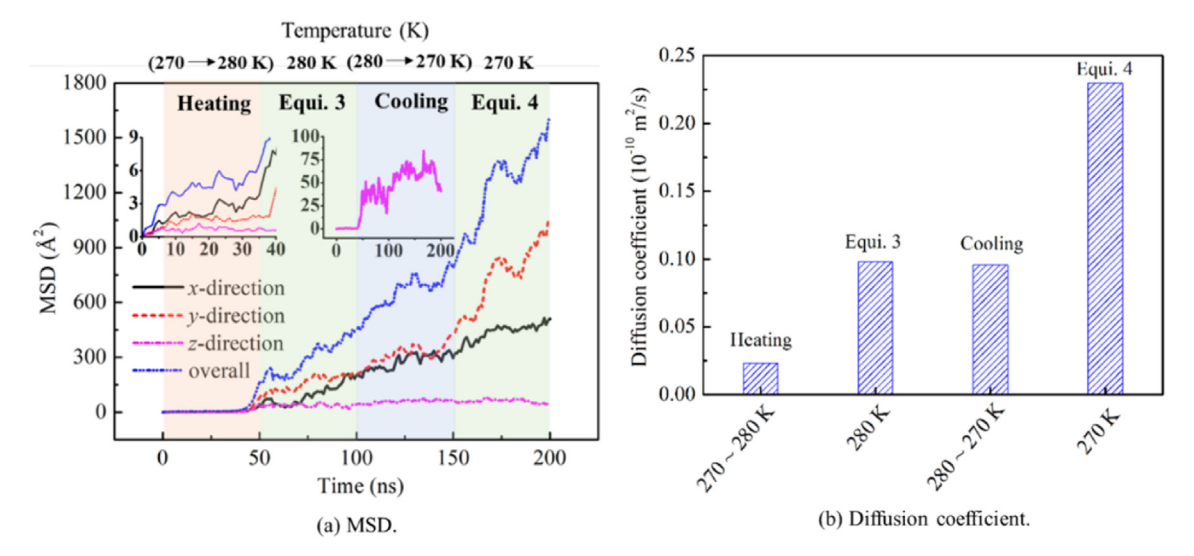


Fig. 14. Evolution of (a) MSD of cation atom (Na⁺) with time, and (b) relationship between its diffusion coefficient (10⁻¹⁰ m²/s) and temperature during heating and cooling process.

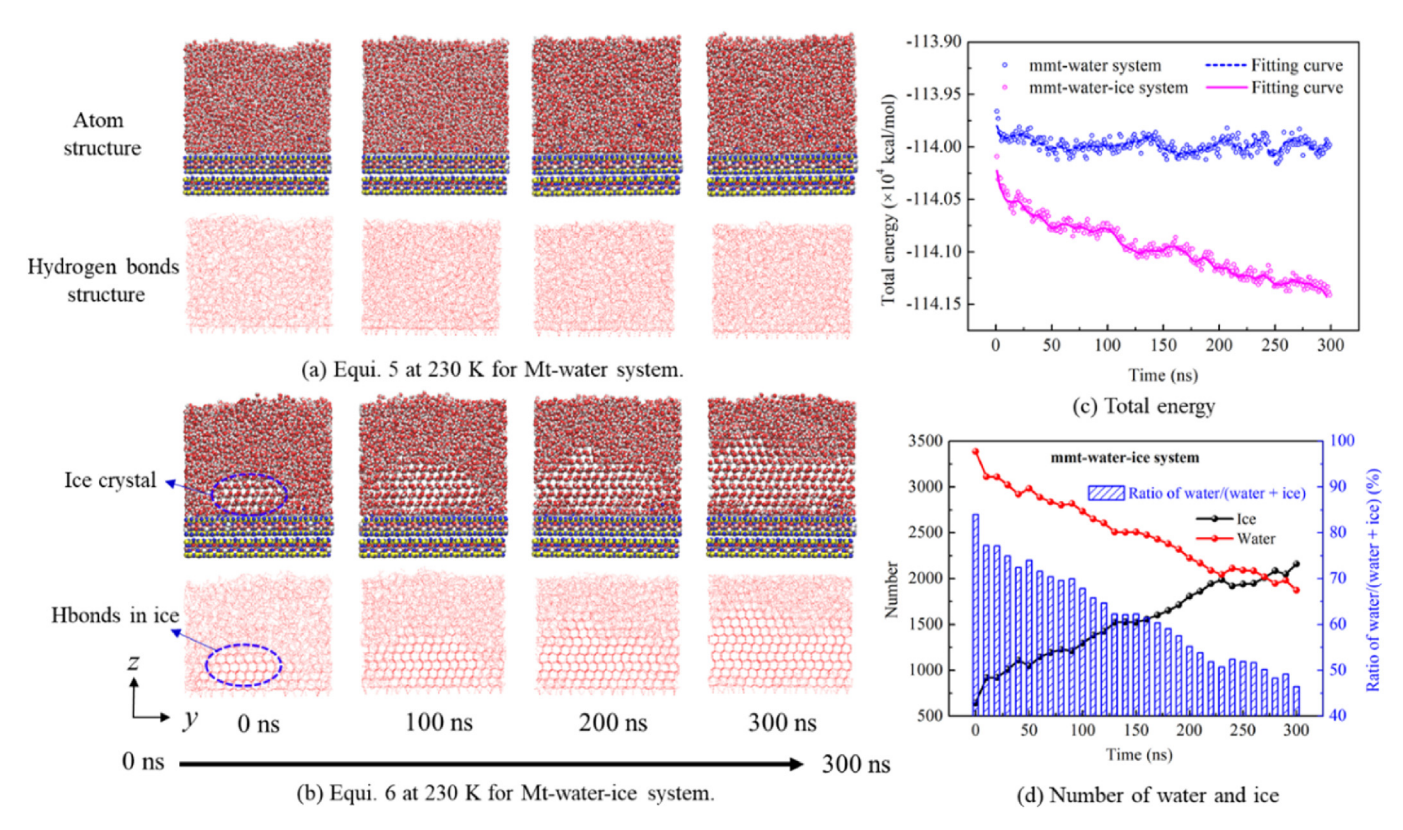


Fig. 15. Atom structure of each system and hydrogen bond structure diagram at 230 K and different simulation time (0–300 ns): (a) Mt-water system without ice and (b) Mt-waterice system, (c) relationship between the total energy of two different systems and time, and (d) relationship between the number of ice and water molecules, the ratio of water/ (water + ice), and time for Mt-water-ice system.

with liquid water properties, such as certain liquidity (Fig. 9a–c) and its density of around 1.0 g/cm³ (Fig. 12d and e). Thus, for unsaturated frozen soil, the unfrozen water included quasi-liquid water on ice surface near air and bound water. The presence of quasi-liquid water significantly impacted the freeze-thaw behavior, water migration, and heat transfer characteristics of frozen soil, which was worth further studying. For saturated frozen soil without air (Region B) (Jin et al., 2020), divided the microstructure

of saturated frozen soil according to an electrical double layer, which does not contain quasi-liquid water. The ice-water phase transition evolution in saturated clay nanopores without air was worth exploring in future. However, for unsaturated frozen soil, we propose a new division of microstructure of unfrozen water and ice on clay particles (Fig. 19b).

The MD results (Fig. A2a) show that even at 210 K, there is at least one layer of bound water adsorbed on the clay surface. This

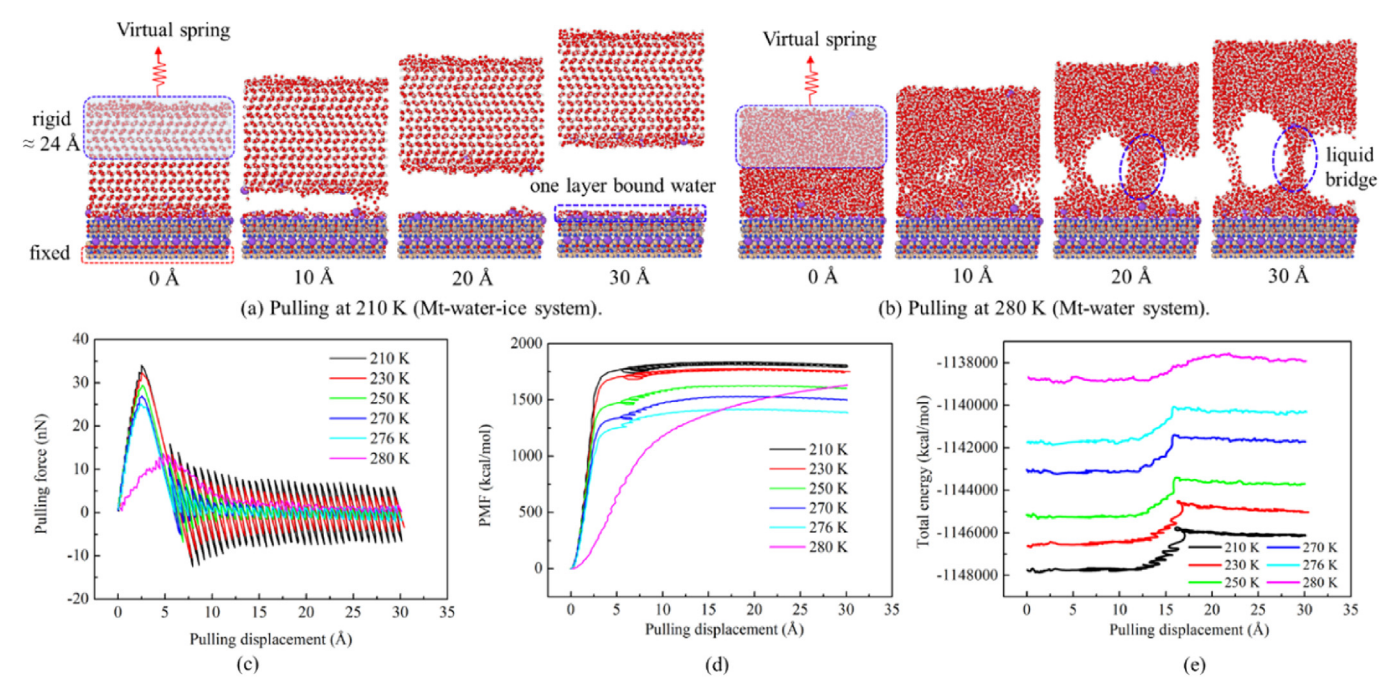


Fig. 16. (a) For Mt-water-ice system under pulling along *z*-direction at 210 K, the atoms in the upper layer are set as rigid (around 24 Å of its constant thickness) and attached to a virtual spring, and the atoms in the lower layer are fixed in their position. (b) Mt-water system without ice under pulling along *z*-direction at 280 K. Evolution of (c) pulling force, (d) potential mean force (PMF), and (e) total energy with pulling displacement at different temperatures of 210–280 K.

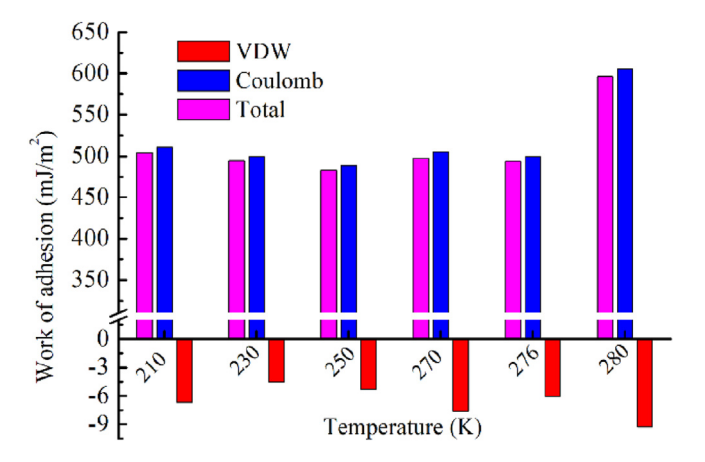


Fig. 17. The work of adhesion (mJ/m²) was calculated through Eq. (4), based on the total potential energy of Mt-water-ice, Mt, and water-ice film systems at different temperatures. Moreover, the contributions from van der Waals (VDW) and coulomb electrostatic interactions are determined, where their calculating equations are similar to Eq. (4).

was due to the surface effect of the clay particles and cations, and it is the main reason for the presence of unfrozen water in frozen soil at ultra-low temperatures, such as 213 K (Figs. 5c) and 193 K (Ren et al., 2023a) in the NMR experiment. For the surface effect of clay, it is found that coulomb electrostatic interaction is dominant, and van der Waals interaction is relatively weak (Fig. 17). Moreover, with rising temperature, the thickness of bound water could increase to 2–3 layers (Fig. 6a–c and A3a). This is consistent with experimental work (Anderson and Hoekstra, 1965), which reported that 2–3 layers of liquid water (i.e. unfrozen water) existing between Wyoming bentonite layers do not freeze below 263 K by X-ray diffractometer. Furthermore, the surface effect of clay is

essential for formation of the bound water (Fig. 18b and c) and ice nucleation (Fig. 15b).

4.4. NMR and MD simulations

The quantitative correlation observed between the MD simulations and NMR experiments underscored the effectiveness of the combined approach in elucidating the freeze-thaw mechanism of montmorillonite clay. Both methods exhibited a consistent trend in unfrozen water content with temperature, highlighting an exponential increase in the severe and transitional phase-transition zones and stability in the freezing stable zone. This agreement could validate the accuracy of the MD simulations in capturing the atomic-level essence of the process. Furthermore, the consistent revelation of the freezing-thawing hysteresis phenomenon by both methods demonstrated MD simulations' capability to capture complex phase transition dynamics. The NMR experiments served as an essential validation of the MD simulations, providing confidence in the accuracy of the models and force fields used. Additionally, the NMR experiments offered unique insights into the different types of unfrozen water present, which was crucial for understanding the hydrological behavior of soil and validated the ability of MD simulation to distinguish water phases. NMR experiments provided macroscopic insights, and MD simulations offered a detailed atomic-level view of the underlying mechanisms, including hydrogen bond evolution, ice nucleation and growth, and surface effects of clay minerals on water-ice interactions. The complementary nature of these two methods could allow for a comprehensive understanding of the freeze-thaw process across different scales. To sum up, the combination of NMR experiments and MD simulations could provide a robust multiscale approach to investigating the freeze-thaw mechanism, with quantitative agreement and unique insights from each method underscoring the value of this integrated strategy.

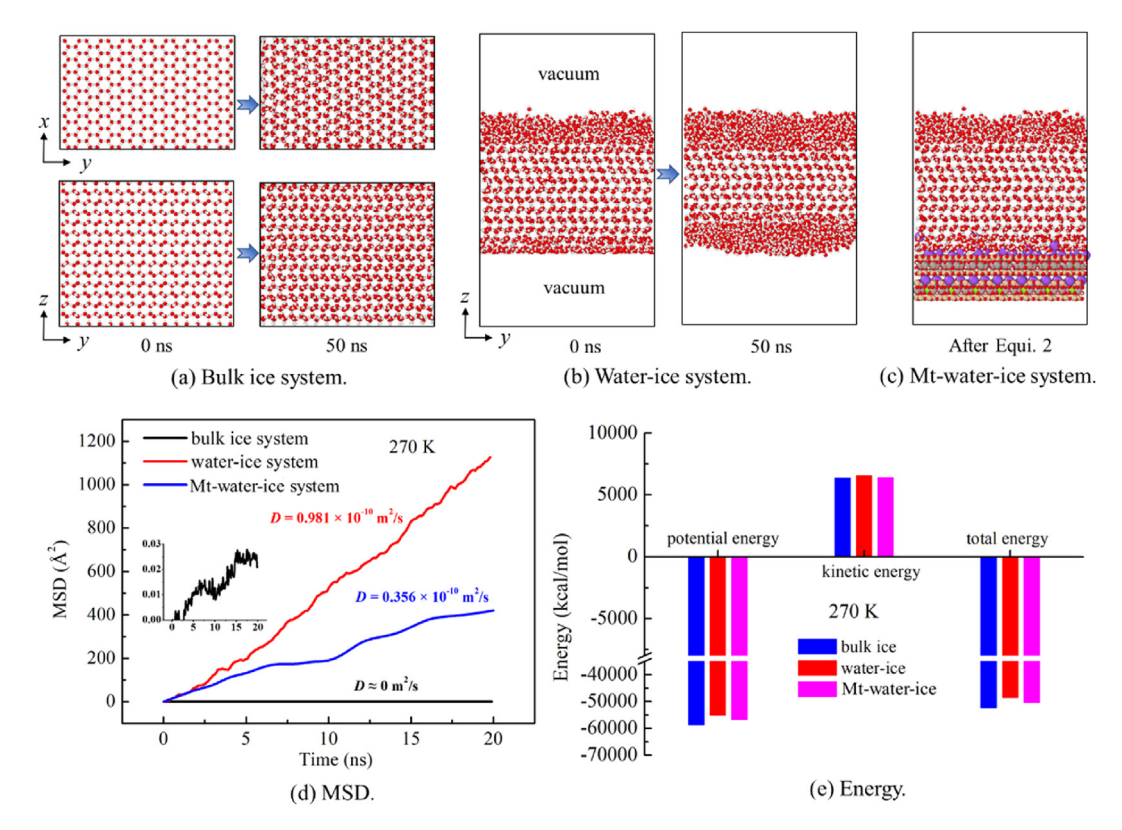


Fig. 18. The structure diagram of different models: (a) bulk ice system under three-dimensional (3D) periodic boundary, (b) water-ice system with vacuum along z-direction, (c) Mt-water-ice system with vacuum, (d) relationship between MSD, diffusion coefficient (D) of O_{TIP4P/ICE} in three different systems, and time during last 20 ns at 270 K, and (e) energy terms (potential, kinetic, and total energy) of ice-(water) in three systems at 270 K.

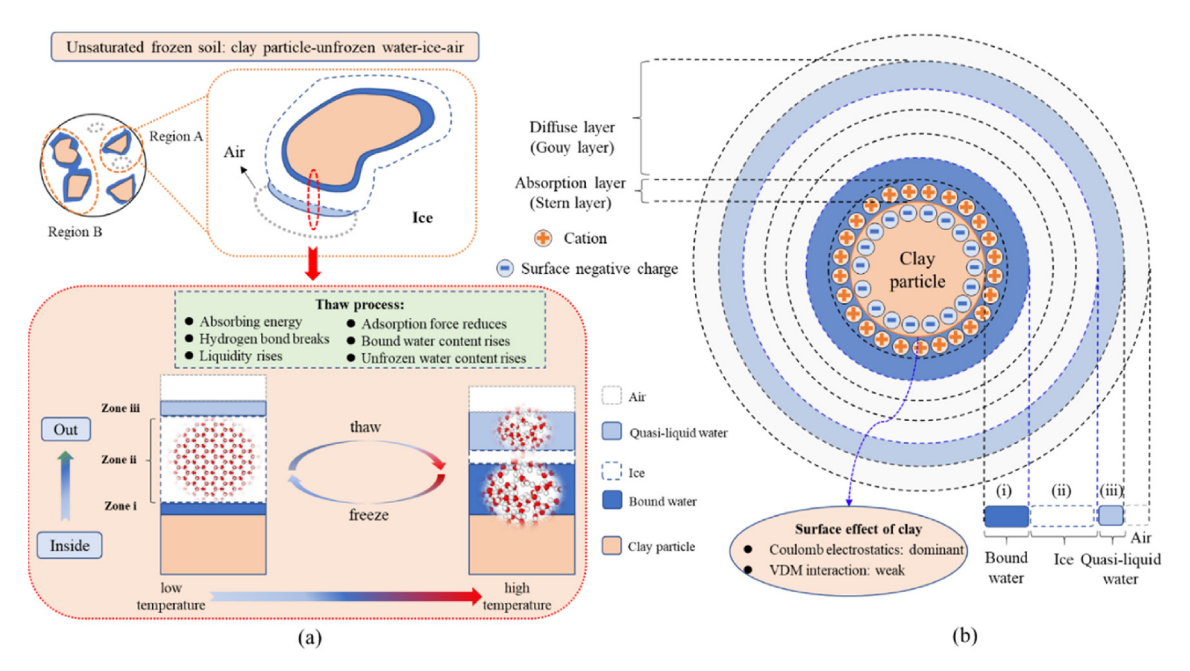


Fig. 19. Division and distribution of unfrozen water and ice microstructure on clay particles below melting temperature: (a) from inside to out, and (b) based on the electrical double layer. Diagram partially developed after (Jin et al., 2020).

5. Conclusions

The nuclear magnetic resonance (NMR) experiment was performed to study the unfrozen water evolution and phase composition in frozen soil at ultra-low temperature (~210 K), and all-atom MD simulation method was applied to unravel their fundamental freeze-thaw mechanism. The conclusions of this study were as follows:

- (1) The evolution of unfrozen water with temperature in MD simulation was consistent with NMR experiment. The freeze-thaw process of frozen soil at the macroscale was essentially the occurrence of ice-water phase transition at the microscale, where the formation and fracture of hydrogen bonds constantly developed with temperature variation at the atomic level.
- (2) The existence of freezing-thawing hysteresis found in MD simulations and NMR experiment was due to different growth and melting rates of ice crystals during freeze-thaw process, where ice growth/nucleation on clay surface needed higher requirements, causing that the water transforming into ice during the freezing process was more difficult than the ice transforming into water during the thawing process.
- (3) A classification method of different types of unfrozen water through NMR experiment was proposed, where the bulk, capillary, and bound water existed in frozen soil at over 270 K was found. Moreover, the gravitational water completely froze at 270 K, capillary water at 268K, and only bound water remained unfrozen below 263 K.
- (4) For unsaturated frozen soil, we proposed a new division of microstructure of unfrozen water and ice on clay particles based on double layer theory. The unfrozen water also contained quasi-liquid water, which was often overlooked in frozen soil mechanics. For saturated frozen soil, the freezethaw mechanism in saturated clay nanopores without air will be worth exploring. On the other hand, the existence of quasi-liquid water layers on ice surface on Mars has not yet been determined, because of significant differences in atmospheric composition, pressure, and temperature between Mars and Earth. Due to the same types of minerals, it can be inferred that there might be a thin layer of bound water (around 3–9 Å) on minerals surface on Mars, which was worth further exploring.

CRediT authorship contribution statement

Pengchang Wei: Conceptualization, Methodology, Investigation, Data Curation, Writing — review & editing, Writing — original draft, Visualization. **Zhen-Yu Yin:** Investigation, Writing — review & editing, Supervision, Project administration. **Chi Yao:** Methodology, Investigation, Writing — review & editing. **Zhifeng Ren:** Conceptualization, Methodology, Investigation, Data Curation, Writing — review & editing, Writing — original draft, Project administration. **Yuan-Yuan Zheng:** Conceptualization, Writing — review & editing, Supervision, Project administration. **Wei Ma:** Data Curation, Methodology.

Data availability statement

The Source data (i.e. MD models) used in this study could be obtained from https://github.com/weipc3/MD-models-for-Atomistic-Origin-of-Freeze-thaw-Mechanism-of-Montmorillonite-Clay.

Code availability statement

The analysis codes (i.e. calculating script in Lammps) used in this study could be obtained from https://github.com/weipc3/MD-code-for-Atomistic-Origin-of-Freeze-thaw-Mechanism-of-Montmorillonite-Clay.

Declaration of competing interest

The authors declare that they have no known competing financial interests or personal relationships that could have appeared to influence the work reported in this paper.

Acknowledgments

This research was financially supported by the Open Fund of State Key Laboratory of Frozen Soil Engineering (Grant No. SKLFSE202104), the Natural Science Foundation of GuangDong Basic and Applied Basic Research Foundation (Grant No. 2024A1515011853), and the Research Grants Council (RGC) of Hong Kong Special Administrative Region Government (HKSARG) of China (Grant Nos.: N_PolyU534/20).

Appendix A. Supplementary data

Supplementary data to this article can be found online at https://doi.org/10.1016/j.jrmge.2024.11.004.

References

- Abascal, J.L.F., Sanz, E., García Fernández, R., Vega, C., 2005. A potential model for the study of ices and amorphous water: tip4p/ice. J. Chem. Phys. 122 (23), 234511. https://doi.org/10.1063/1.1931662.
- Al-Zaoari, K., Zheng, Y., Wei, P., Zhang, L., Yin, Z., 2022. Early stage of swelling process of dehydrated montmorillonite through molecular dynamics simulation. Mater. Chem. Phys. 283, 126015. https://doi.org/10.1016/ j.matchemphys.2022.126015.
- Anderson, D.M., Hoekstra, P., 1965. Migration and Crystallization of Interlamellar Water during Freezing and Thawing of wyoming Bentonite. Research Report -Corps of Engineers, U. S. Army, Cold Regions Research and Engineering Laboratory. https://doi.org/10.2136/sssaj1965.03615995002900050010x.
- Anderson, D.M., Tice, A.R., 1972. Predicting Unfrozen Water Contents in Frozen Soils from Surface Area Measurements. Highway Research Record.
- Asuri, S., Keshavamurthy, P., 2016. Expansive soil characterisation: an appraisal. INAEL 1 (1), 29–33. https://doi.org/10.1007/s41403-016-0001-9.
- Bai, G., Gao, D., Liu, Z., Zhou, X., Wang, J., 2019. Probing the critical nucleus size for ice formation with graphene oxide nanosheets. Nature 576 (7787), 437–441. https://doi.org/10.1038/s41586-019-1827-6.
- Bernal, J.D., Fowler, R.H., 1933. A theory of water and ionic solution, with particular reference to hydrogen and hydroxyl ions. J. Chem. Phys. 1 (8), 515–548. https://doi.org/10.1063/1.1749327.
- Birgersson, M., Karnland, O., Nilsson, U., 2010. Freezing of bentonite. Experimental Studies and Theoretical Considerations. Sweden.
- Blazquez, S., Vega, C., 2022. Melting points of water models: current situation. J. Chem. Phys. 156 (21), 216101. https://doi.org/10.1063/5.0093815.
- Chen, Y., Zhou, Z., Wang, J., Zhao, Y., Dou, Z., 2021. Quantification and division of unfrozen water content during the freezing process and the influence of soil properties by low-field nuclear magnetic resonance. J. Hydrol. 602, 126719. https://doi.org/10.1016/j.jhydrol.2021.126719.
- Clancy, T.C., Mattice, W.L., 1999. Computer simulation of polyolefin interfaces. Comput. Theor. Polym. Sci. 9 (3–4), 261–270. https://doi.org/10.1016/S1089-3156/99)00013-6
- Cox, S.J., Raza, Z., Kathmann, S.M., Slater, B., Michaelides, A., 2014. The microscopic features of heterogeneous ice nucleation may affect the macroscopic morphology of atmospheric ice crystals. Faraday Discuss 167, 389. https://doi.org/10.1039/c3fd00059a.
- Cygan, R.T., Liang, J., Kalinichev, A.G., 2004. Molecular models of hydroxide, oxyhydroxide, and clay phases and the development of a general force field. J. Chem. Phys. B 108 (4), 1255–1266. https://doi.org/10.1021/jp0363287.
- Du, P., Yuan, P., Liu, J., Ye, B., 2023. Clay minerals on mars: an up-to-date review with future perspectives. Earth Sci. Rev. 243, 104491. https://doi.org/10.1016/ j.earscirev.2023.104491.
- Frenkel, D., Smit, B., 2001. Understanding Molecular Simulation: from Algorithms to Applications. Academic Press. http://doi.org/10.1016/B978-012267351-1/50012-2.

- Furukawa, Y., Yamamoto, M., Kuroda, T., 1987. Ellipsometric study of the transition layer on the surface of an ice crystal. J. Cryst. Growth 82 (4), 665–677. https://doi.org/10.1016/S0022-0248(87)80012-X.
- García Fernández, R., Abascal, J.L.F., Vega, C., 2006. The melting point of ice ih for common water models calculated from direct coexistence of the solid-liquid interface. J. Chem. Phys. 124 (14), 144506. https://doi.org/10.1063/1.2183308.
- Jin, X., Yang, W., Gao, X., Zhao, J.Q., Li, Z., Jiang, J., 2020. Modeling the unfrozen water content of frozen soil based on the absorption effects of clay surfaces. Water Resour. Res. 56 (12), https://doi.org/10.1029/2020WR027482.
- Kawakami, N., Iwata, K., Shiotari, A., Sugimoto, Y., 2020. Intrinsic reconstruction of ice-i surfaces. Sci. Adv. 6 (37). https://doi.org/10.1126/sciadv.abb7986.
- Kong, L., Wang, Y., Sun, W., Qi, J., 2020. Influence of plasticity on unfrozen water content of frozen soils as determined by nuclear magnetic resonance. Cold Reg. Sci. Technol. 172, 102993. https://doi.org/10.1016/j.coldregions.2020.102993.
- Li, K., Yin, Z., 2024. State of the art of coupled thermo—hydro-mechanical—chemical modelling for frozen soils. Arch. Comput. Method. E. https://doi.org/10.1007/s11831-024-10164-w
- Li, X., Li, X., Liu, J., 2023. A dynamic soil freezing characteristic curve model for frozen soil. J. Rock Mech. Geotech. https://doi.org/10.1016/j.jrmge.2023.09.008. Liang, T., Lai, Y., Hou, D., Pei, W., Wang, M., Yu, F., Yang, Q., Yang, Y., Li, H., 2023.
- Liang, T., Lai, Y., Hou, D., Pei, W., Wang, M., Yu, F., Yang, Q., Yang, Y., Li, H., 2023. Molecular dynamics simulation investigation on the anti-freezing mechanisms of csh-gs/go interfaces. Construct. Build. Mater. 369, 130581. https://doi.org/ 10.1016/j.conbuildmat.2023.130581.
- Liu, Y., Zheng, Y., Lin, H., Wei, P., Fan, Q., Huang, G., Meng, D., 2024. Calculation of contact angle via Young-Dupré equation with molecular dynamic simulation: Kaolinite as an example. Colloids Surf., A 697, 134469. https://doi.org/10.1016/ j.colsurfa.2024.134469.
- Maras, E., Trushin, O., Stukowski, A., Ala-Nissila, T., Jónsson, H., 2016. Global transition path search for dislocation formation in ge on si(001). Comput. Phys. Commun. 205, 13–21. https://doi.org/10.1016/j.cpc.2016.04.001.
- Matsumoto, M., Saito, S., Ohmine, I., 2002. Molecular dynamics simulation of the ice nucleation and growth process leading to water freezing. Nature 416. https:// doi.org/10.1038/416409a.
- Mironov, V.L., Karavayskiy, A.Y., Lukin, Y.I., Pogoreltsev, E.I., 2018. Joint studies of water phase transitions in na-bentonite clay by calorimetric and dielectric methods. Cold Reg. Sci. Technol. 153, 172–180. https://doi.org/10.1016/ j.coldregions.2018.04.010.
- Nan, J., Liu, J., Chang, D., Li, X., 2022. Mechanical characteristics and microstructure study of saline soil stabilized by quicklime after curing and freeze-thaw cycle. Cold Reg. Sci. Technol. 201, 103625. https://doi.org/10.1016/ j.coldregions.2022.103625.
- Niu, W., Liu, J., Kravchenko, E., Zheng, Y., Tai, B., Wei, P., 2024. Mechanical properties of subgrade soil reinforced with basalt fiber and cement under freeze—thaw cycles. J. Mater. Civ. Eng. 36 (12), 04024398. https://doi.org/10.1061/JMCEE7.MTENG-17161.
- Pan, Z., Zhou, K., Gao, R., Jiang, Z., Yang, C., Gao, F., 2020. Research on the pore evolution of sandstone in cold regions under freeze-thaw weathering cycles based on nmr. Geofluids 1–12. https://doi.org/10.1155/2020/8849444, 2020.
- Plimpton, S., 1995. Fast paraller algorithms for short-range molecular dynamics. J. Comput. Phys. 117, 1–19. https://doi.org/10.1006/jcph.1995.1039.
- Qiu, B., Fan, L., Du, X., 2024. Microstructure deterioration of sandstone under freezethaw cycles using ct technology: the effects of different water immersion conditions. J. Rock Mech. Geotech. https://doi.org/10.1016/j.jrmge.2024.02.002.
- Ren, Z., Liu, J., Jiang, H., Wang, E., 2023a. Experimental study and simulation for unfrozen water and compressive strength of frozen soil based on artificial freezing technology. Cold Reg. Sci. Technol. 205, 103711. https://doi.org/10.1016/ j.coldregions.2022.103711.
- Ren, Z., Wang, E., Liu, J., Jiang, H., Yao, Z., 2023b. Characterization and prediction of compressive strength in ultralow-temperature frozen soil using nuclear magnetic resonance and woa-enn model. Transp. Geotech. 43, 101143. https:// doi.org/10.1016/j.trgeo.2023.101143.
- Sebastián, E., Armiens, C., Gómez-Elvira, J., Zorzano, M.P., Martinez-Frias, J., Esteban, B., Ramos, M., 2010. The rover environmental monitoring station ground temperature sensor: a pyrometer for measuring ground temperature on mars. Sensors-Basel 10 (10), 9211–9231. https://doi.org/10.3390/s101009211.
- Shi, B., Jiang, H., Liu, Z., Fang, H.Y., 2002. Engineering geological characteristics of expansive soils in China. Eng. Geol. 67 (1–2), 63–71. https://doi.org/10.1016/ S0013-7952(02)00145-X.
- Smit, W.J., Bakker, H.J., 2017. The surface of ice is like supercooled liquid water. Angew. Chem. 129 (49), 15746–15750. https://doi.org/10.1002/ange.201707530.
- Sosso, G.C., Li, T., Donadio, D., Tribello, G.A., Michaelides, A., 2016a. Microscopic mechanism and kinetics of ice formation at complex interfaces: zooming in on kaolinite. J. Phys. Chem. Lett. 7 (13), 2350–2355. https://doi.org/10.1021/ acs.joclett.6b01013.
- Sosso, G.C., Tribello, G.A., Zen, A., Pedevilla, P., Michaelides, A., 2016b. Ice formation on kaolinite: insights from molecular dynamics simulations. J. Chem. Phys. 145 (21), 211927. https://doi.org/10.1063/1.4968796.
- Stukowski, A., 2010. Visualization and analysis of atomistic simulation data with ovito—the open visualization tool. Model. Simul. Mater. Sc. 18 (1), 015012. https://doi.org/10.1088/0965-0393/18/1/015012.

- Svensson, P.D., Hansen, S., 2010. Freezing and thawing of montmorillonite a time-resolved synchrotron x-ray diffraction study. Appl. Clay Sci. 49 (3), 127–134. https://doi.org/10.1016/j.clay.2010.04.015.
- Tian, H., Wei, C., Wei, H., Zhou, J., 2014. Freezing and thawing characteristics of frozen soils: bound water content and hysteresis phenomenon. Cold Reg. Sci. Technol. 103, 74–81. https://doi.org/10.1016/j.coldregions.2014.03.007.
- Tsytovich, N.A., 1975. In: Swinzow, G.K., Swinzow, G.K. (Eds.), The Mechanics of Frozen Ground. McGraw-Hill Book Co, New York, N. Y.
- Tulk, C.A., Molaison, J.J., Makhluf, A.R., Manning, C.E., Klug, D.D., 2019. Absence of amorphous forms when ice is compressed at low temperature. Nature 569 (7757), 542–545. https://doi.org/10.1038/s41586-019-1204-5.
- Viani, A., Gualtieri, A.F., Artioli, G., 2002. The nature of disorder in montmorillonite by simulation of x-ray powder patterns. Am. Mineral. 87, 966–975. https:// doi.org/10.2138/am-2002-0720.
- Wang, J., Cui, D., Chen, Q., Chen, J., Dai, M., 2023. Morphological damage and strength deterioration of red sandstone under freezeethaw cycles. J. Rock Mech. Geotech. https://doi.org/10.1016/j.jrmge.2023.09.022.

 Wang, Y., Hu, L., 2023. A theoretical model of soil freezing characteristic curve
- Wang, Y., Hu, L., 2023. A theoretical model of soil freezing characteristic curve considering the freezing of adsorbed water and capillary water. Water Resour. Res. 59 (7), https://doi.org/10.1029/2023WR034662.
- Weber, B., Nagata, Y., Ketzetzi, S., Tang, F., Smit, W.J., Bakker, H.J., Backus, E.H.G., Bonn, M., Bonn, D., 2018. Molecular insight into the slipperiness of ice. J. Phys. Chem. Lett. 9 (11), 2838–2842. https://doi.org/10.1021/acs.jpclett.8b01188.
- Wei, P., Zhuang, D., Zheng, Y., Zaoui, A., Ma, W., 2022a. Temperature and pressure effect on tensile behavior of ice-ih under low strain rate: a molecular dynamics study. J. Mol. Liq. 355, 118945. https://doi.org/10.1016/j.molliq.2022.118945.
- Wei, P., Zheng, Y., Xiong, Y., Zhou, S., Al-Zaoari, K., Zaoui, A., 2022b. Effect of water content and structural anisotropy on tensile mechanical properties of montmorillonite using molecular dynamics. Appl. Clay Sci. 228, 106622. https:// doi.org/10.1016/j.clay.2022.106622.
- Wei, P., Zheng, Y., Zaoui, A., Ma, W., Ren, Z., 2024a. Ice-unfrozen water on mont-morillonite surface: a molecular dynamics study. Geomech. Energy Envir. 39, 100569. https://doi.org/10.1016/j.gete.2024.100569.
- Wei, P., Zheng, Y., Zaoui, A., 2024b. Frictional mechanisms of hydrated montmorillonite under normal loading. Comput. Geotech. 173, 106568. https://doi.org/ 10.1016/j.compgeo.2024.106568.
- Wei, P., Zhou, S., Zheng, Y., Yin, Z., Xu, W., 2024c. Nanoscale Stick-Slip behavior and hydration of hydrated illite clay. Comput. Geotech. 166, 105976. http://doi.org/ 10.1016/j.compgeo.2023.105976.
- Wu, T., Li, H., Lyu, H., 2023. Effect of freeze—thaw process on heat transfer and water migration between soil water and groundwater. J. Hydrol. 617, 128987. https:// doi.org/10.1016/j.jhydrol.2022.128987.
- Yang, W., Zaoui, A., 2016. Capture and sequestration of co2 in the interlayer space of hydrated calcium montmorillonite clay under various geological burial depth. Phys. A 449, 416–425. https://doi.org/10.1016/j.physa.2015.12.032.
- Zhang, C., Liu, Z., Deng, P., 2018. Using molecular dynamics to unravel phase composition behavior of nano-size pores in frozen soils: does young—laplace equation apply in low temperature range? Can. Geotech. J. 55 (8), 1144—1153. https://doi.org/10.1139/cgj-2016-0150.
- Zhang, L., Zaoui, A., Sekkal, W., Zheng, Y., 2023. Interlayer adsorption of cationic dye on cationic surfactant-modified and unmodified montmorillonite. J. Hazard Mater. 442, 130107. https://doi.org/10.1016/j.jhazmat.2022.130107.
- Zhang, S., Pei, H., 2021. Determining the bound water content of montmorillonite from molecular simulations. Eng. Geol. 294, 106353. https://doi.org/10.1016/ j.enggeo.2021.106353.
- Zhao, G., Zou, W., Han, Z., Wang, D., Wang, X., 2021. Evolution of soil-water and shrinkage characteristics of an expansive clay during freeze-thaw and dryingwetting cycles. Cold Reg. Sci. Technol. 186, 103275. https://doi.org/10.1016/ j.coldregions.2021.103275.
- Zheng, Y., Zaoui, A., 2018. Mechanical behavior in hydrated na-montmorillonite clay. Phys. A 505, 582–590. https://doi.org/10.1016/j.physa.2018.03.093.
- Zielke, S.A., Bertram, A.K., Patey, G.N., 2016. Simulations of ice nucleation by kaolinite (001) with rigid and flexible surfaces. J. Chem. Phys. B 120 (8), 1726–1734. https://doi.org/10.1021/acs.jpcb.5b09052.



Yuan-Yuan Zheng obtained her BSc degree in water conservancy and hydropower construction engineering from Hohai University, China in 2002. She received her MSc and PhD at University of Lille, France in 2005 and 2010, respectively. She took the position of lecturer, associate professor at the same university. She then joined the School of Civil Engineering at Sun Yat-Sen University (China) in 2018. She is engaged in research on nanoscale modeling and molecular dynamics simulation study of clay minerals and civil engineering materials.